Automated Docking of an Offshore Gangway

A Predictive Control Approach

M. A. Ranneh

Master of Science Thesis

TU Delft Delft University of Technology

Delft Center for Systems and Control

Automated Docking of an Offshore Gangway

A Predictive Control Approach

Master of Science Thesis

For the degree of Master of Science in Systems and Control at Delft University of Technology

M. A. Ranneh

June 29, 2019

Faculty of Mechanical, Maritime and Materials Engineering (3mE) · Delft University of Technology

The work in this thesis was supported by Bosch Rexroth. Their cooperation is hereby gratefully acknowledged.

Delft University of Technology
Department of
Delft Center for Systems and Control (dcsc)

The undersigned hereby certify that they have read and recommend to the Faculty of Mechanical, Maritime and Materials Engineering (3mE) for acceptance a thesis entitled

Automated Docking of an Offshore Gangway

by

M. A. Ranneh

in partial fulfillment of the requirements for the degree of

Master of Science Systems and Control

Dated: June 29, 2019

Supervisor(s):

Dr.ir. E. Steur

Ir. M.J. van de Molengraft

Reader(s):

Prof.dr.ir. B. De Schutter

Dr.ir. K. Batselier

Abstract

Objects floating on or near the water surface (e.g. vessels, and floating wind-turbines) suffer from motions induced by waves of varying height, direction, and frequency. This not only causes unpleasantness for passengers and crew of ships but also it limits the accessibility to the offshore platforms. Bosch Rexroth with their partner Barge Master have developed the so-called Motion Compensated Gangway that provides a safe passage for cargo and personnel to offshore structures.
In order to maintain a motionless connection with the offshore structure, once the tip of the gangway is pushed against the offshore structure. The gangway system actively compensates for the sea-induced motion that acts on the vessel.
However, the docking procedure is still manually attained, where accidents may occur due to human error (i.e. insufficient training, loss of concentration). One way to improve the current control scheme is to enable an automated docking scheme.
Accordingly, the main of this project focuses on eliminating the human factor from the control loop, so the overall process is accomplished automatically and more efficiently in terms of safety and performance.
Inspired by how the operator estimates the relative motion between the Gangway and the target (i.e. the offshore platform). In this thesis, a measurement system is proposed to measure this relative motion. This measurement system comprises a vision sensor, force tip measurements, and Motion Reference Unit (MRU). In this thesis, the proposed automated docking scheme is developed around a nonlinear MPC scheme. For the simulation environment and for the MPC scheme employs, a nonlinear model of the gangway system is derived. This model embeds an approximation of the joint-level control loop of the Gangway system. Also, this model comprises the open-chain kinematic model of the Gangway system and the proposed measurement system including a perspective projection model of the vision sensor. Due to modelling the vision sensor as such and the MPC's capability in handling various constraints, the proposed control scheme enjoys a singularity-free solution.
The proposed control scheme detects and tracks the target in the 2D image plane. To safeguard against visual measurements discontinuity (i.e. cluttering, target outside the field of view), a linear Kalman filter is designed to predict the target position in the image plane.
To gain higher performance, the disturbance anticipatory property in MPC is enabled by

forecasting the sea-induced motion. Where a neural network with the NARX topology was designed and trained to acquire a multi-step-ahead prediction model of the induced motion. Several numerical experiments were carried to evaluate the performance of the proposed control scheme for automated docking. Where for the nominal case scenarios all the control requirements are fulfilled. Also, more extreme scenarios are performed to evaluates the overall performance under plant model mismatch and against various sea-induced motion conditions. Evidently, the proposed control scheme is prone to camera calibrations error.
In terms of the efficiency, the proposed automated docking scheme performs the docking in 4 to 10 seconds (based on the initial conditions and sea state). Whereas the time it takes the operator to perform the docking is up to 3 minutes which depends on his/her experience.

Table of Contents

List of Figures

List of Tables

Acknowledgements

First and foremost, I would like to praise God for his blessings and for giving me this wonderful opportunity - to be part of this master program.

I would like to thank my supervisor at TU Delft, Dr. Erik Steur, for his adequate supervision throughout my master's thesis project, and for teaching me to be critical and organised in my work.
I would also like to thank my supervisor at Bosch, Ir. Maik van de Molengraft, for his excellent guidance and support on both technical and personal levels.

Last but not least, I want to express my gratitude for my parents who dedicated their lives to bring the best out of me, while never stopped offering their unwavering support.

Delft, University of Technology M. A. Ranneh
June 29, 2019

"A year spent in artificial intelligence is enough to make one believe in God."
— *Alan Perlis*

Chapter 1

Introduction

1-1 Background

According to the World Wind Energy Association, the total capacity of wind energy has been significantly increased over the last decade, especially, the offshore sector [1], see Figure 1-1. Offshore wind farms are becoming more favourable since it has many advantages over the onshore wind energy (e.g. less turbulent, more space for larger rotors diameter, higher capacity due to more sustained wind) [1].
However, the enormous costs of construction and maintenance of offshore wind farms introduce a striking increase to the overall cost. Consequently, implementing innovative solutions and mechanisms in the affiliated industrial fields will result in reducing the technical risk and finance costs which will attract more investments.

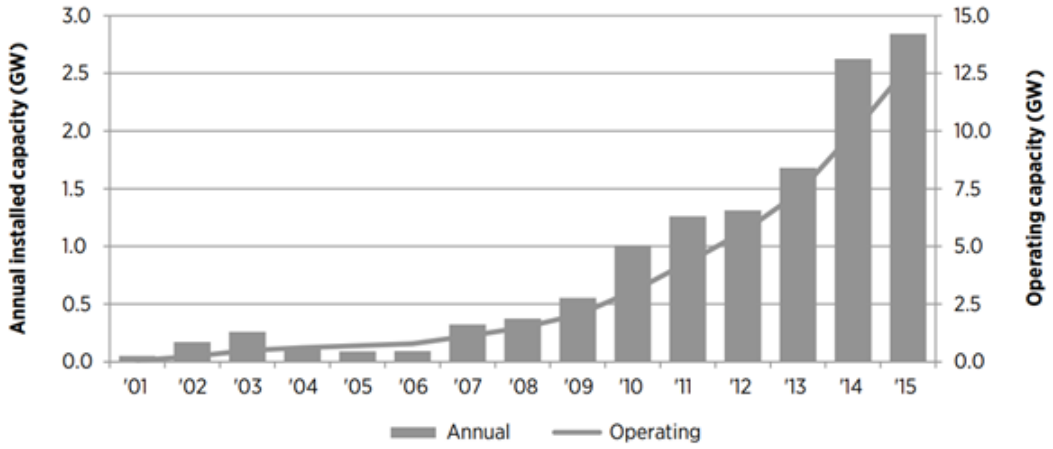

Figure 1-1: Global annual installed capacity and operating capacity of offshore wind between 2001-2015. From [1].

Former methods of personnel and cargo transfer to offshore structures are generally limited to; a helicopter lowering personnel to the structure, cranes with a suspended basket, and a crew transfer boats that push against a landing zone, See Figure 1-2. these methods are rather inefficient in terms of cost, safety, and the operating window [13].
In 2008, the first motion compensated gangway was introduced to the market by Ampelmann [14], which is a gangway attached to the top of a hydraulically actuated Stewart. This was a game changer in the offshore logistics sector. Accordingly, many companies started developing their own motion compensated gangway becoming a highly competitive field which resulted in the lack of related published work in the literature.

(a) **(b)** **(c)**

Figure 1-2: (a) A crane with a suspended basket. (b) A boat bushing onto a monopile. (C) A helicopter lowering personnel on a wind turbine. From [2–4].

Waves of varying height, direction and frequency are constantly present, objects floating on or near the water surface (e.g. ships, vessels, and floating wind-turbines) suffer from motions induced by these waves, this can cause unpleasantness for passengers and crew of ships but can also carry serious risks for both people and equipment in any type of offshore operation. Offshore gangway systems are usually installed on a vessel. The vessel responds to the induced motions via sea state in six Degrees of Freedom Degree of Freedom (DoF); three translations (surge, sway, heave) and three rotations (roll, pitch, yaw). Figure 1-3 illustrates the axes conventions of a vessel.
This type of vessels is supplied with a Dynamic Positioning (DP) system. With the DP system, the vessel can stay in place at a short distance from the offshore structure with relatively small deviations by actively controlling the propellers, rudders and, thrusters. This can only compensate for the occurred movements in the horizontal plane. The gangway system is activated only when the vessel's DP system is enabled.
Consequently, a gangway system has to account mainly for heave motions. However, due to a possible drift error in the DP system, the gangway system also needs to compensate for yaw and sway. It is worth mentioning that roll and pitch movements can be neglected due to the length of and the huge mass of the vessel which can damp out the perturbations on the aforementioned axes. Therefore, with a predefined operating window, along with the DP system, it is safe to argue that a three-DoF structure for an offshore gangway is sufficient. Based on this concept, Bosch Rexroth with their partner Barge Master have developed a Motion Compensated Gangway Motion Compensated Gangway (MCG) that provides a safe passage for cargo and personnel transfer to offshore structures, see Figure 1-4. In this thesis, the configuration and design of Bosch's gangway system will be used for modelling and control design.

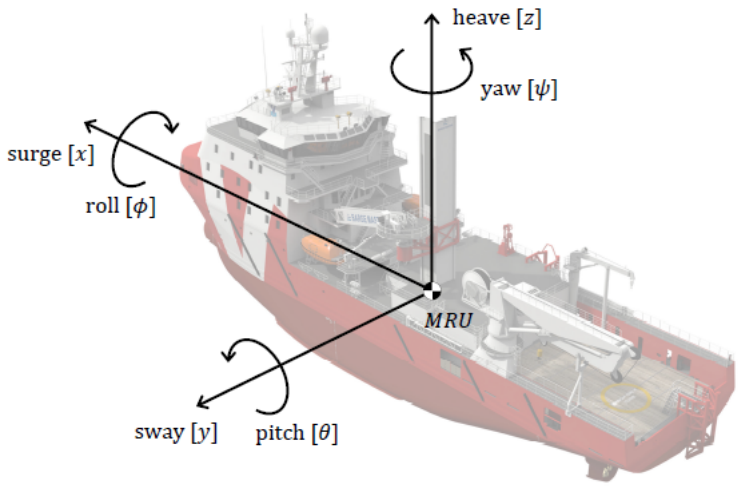

Figure 1-3: The vessel's axes signs and naming conventions. From [5].

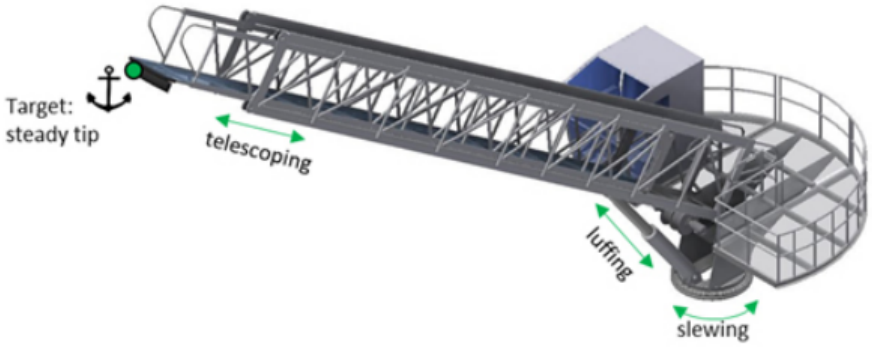

Figure 1-4: The working principle of Bosch's gangway system. From [6].

The word "Gangway" in sentence case will be used throughout this report to refer to Bosch's gangway (Gangway) system.

1-2 Problem statement

At the present time, all existing gangway systems in the market are obliged to employ an operator in their control loop for legal and safety-related issues [15].
Figure 1-5 depicts the high-level scheme of the control system of Bosch's gangway system. The system, through an inertial measurement unit, can automatically counteract the sea-induced motion in a feedforward fashion. The operator function is limited to steer the motion compensated tip of the gangway. The control interface in the gangway system is merely based on three joysticks where each joystick generates the position setpoint for each actuator.
Moreover, the operator's cabin is attached on top of the Gangway base. This means that

he/she perceives the vessel surrounding environment in a non-inertial frame. Because of this, the operator's task in docking the Gangway to the offshore platform becomes challenging and nontrivial. Consequently, the operator must follow excessive training (similar to a crane operating training) in order to be qualified as an offshore gangway operator [15].
Since the docking procedure is manually attained, accidents may occur due to human error (i.e. insufficient training, loss of concentration). One way to improve the current control scheme is to enable an automated docking scheme, which employs range sensing technologies within its measurement system (e.g. radar, lidar, camera, etc.).
Accordingly, the outcome of this project focuses on eliminating the human factor from the control loop, so the overall process is accomplished automatically and more efficiently in terms of safety and performance.

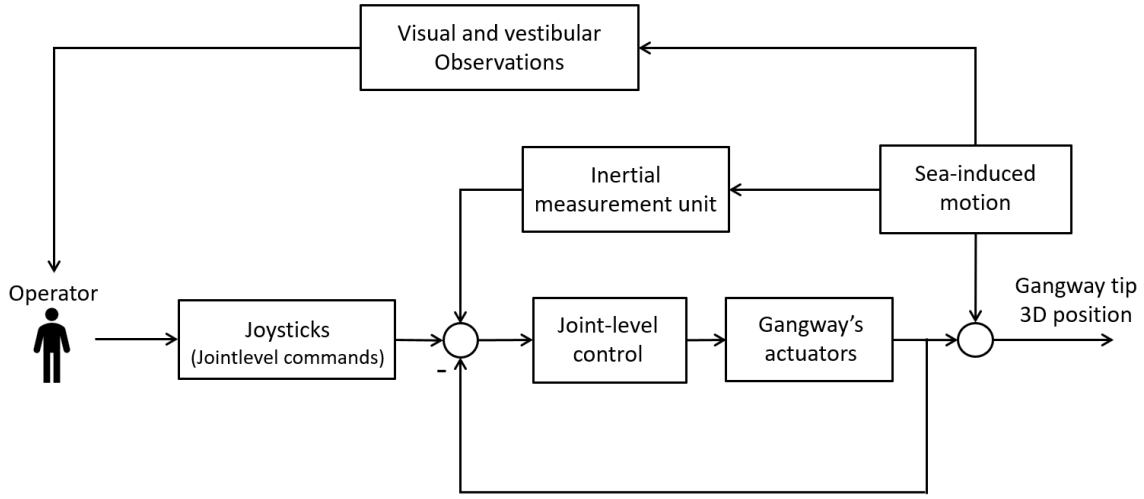

Figure 1-5: A high-level scheme of the control system of Bosch gangway.

1-3 Research Objectives

Enabling the automated docking scheme for the Gangway system corresponds to eliminating the human presence (i.e. the operator) in the control loop.
Thus, the main research objective is to propose a control scheme for docking the Gangway tip onto the offshore platform autonomously while actively compensating for the sea-induced motion.
At the beginning of this project, a literature study was conducted, [16], to create a base of knowledge to assist in the completion of the thesis-project:

"Automated Docking of an Offshore Gangway"

Correspondingly, the research questions were formulated as:

Q1. *What is the architecture and characteristics of the current system? What are the control requirement of the Gangway system?*

Q2. *How to measure the relative motion between the Gangway and the docking area?*

Q3. *What kind of sensing technologies are to be included in the measurement system for the automated docking?*

Q4. *How can a vision sensor be incorporated within the control loop for automated docking?*

Q5. *Is there a control scheme that combines vision and force control while handling constraints?*

Q6. *Is it possible to forecast the sea-induced motion? Would the proposed control method benefit from anticipating the external perturbation ahead?*

1-4 Preliminary assumptions and considerations

In order to answer the research questions, a set of assumptions and operating constraints are set for the system modelling and control design. The following assumptions are made:

- Actuators dynamics are not considered explicitly but rather implicitly. An approximation is provided by Bosch to describe the low-level (joint-level) control loop as a second order system.
- For the sake of simplicity; no deformations occur in both the vertical and torsional axes of the Gangway.
- Relative motion hypothesis: The residual motion of the vessel, which is caused by the sea-induced motion, is slow sinusoidal-based motion. From the operator's point of view (with ignoring his vestibular senses) the sea-induced motion that acts on the vessel causes the target (i.e. offshore platform) to move instead. This assumption is made to describe the Gangway kinematics and dynamics in an inertial frame. This should result in a simpler model which is required by the proposed control strategy.
- Bosch has defined an operation window for which the Gangway system function within:
  - Maximum wind speed: 20 m/sec. The wind speed below this limit does not affect the overall performance of the Gangway system [6].
  - Operating in both daylight and nighttime with sufficient illumination on the gangway tip that is defined by DNV-GL standards [15].
  - The wave period is between 4 and 12 seconds with H_{sig} (the significant wave height) is no more than 3.0 m [6].

1-5 Thesis contributions

In Chapter 3, a measurement system is proposed to measure the relative motion between the Gangway and the offshore platform. This measurement system comprises a vision sensor, force tip measurements, and Motion Reference Unit (MRU). In Chapter 4, a nonlinear Model Predictive Control (MPC) is designed to solve the automated docking problem by utilising

the aforementioned measurement system. Hence, the main contributions of this thesis-project lie in the outcome of Chapter 4. The proposed control scheme enjoys the following:

- Fast docking time (up to 10 seconds) compared to the time it takes the operator to perform the docking (up to 3 minutes) which is dependent on his/her experience [7].
- This control scheme utilises the vision, the induced motion, and tip force measurements in one control scheme to steer and dock the Gangway tip onto the offshore platform. Hence, no need for a switching control scheme.
- This control scheme detects and tracks the target (i.e. the offshore platform) in the 2D image plane. Therefore, the control scheme is prone to camera calibrations error. Additionally, in Chapter 3, a linear Kalman filter is designed to predict the target position in the image plane when if the target leaves the field of view. This can safeguard against visual measurements discontinuity, which might be problematic from a control perspective.
- The proposed scheme is based on nonlinear MPC. Hence, system constraints and its physical limitations can naturally be satisfied.
- To gain higher performance, the disturbance anticipatory property in MPC is enabled by forecasting the sea-induced motion. A neural network with the NARX topology was designed and trained to acquire a multi-step-ahead prediction model of the induced motion.

1-6 Thesis outline

In this chapter, the problem statement and the research objectives of this project are presented along with preliminary research assumptions and considerations. The remainder of this thesis structured as follows:

- **Chapter 2**: System Architecture. This chapter address the research questions Q1 by introducing the Gangway system architecture as designed by Bosch. In terms of its mechanical structure, actuator, and measurement system. Furthermore, the physical limitation and control task requirements of the system are presented.
- **Chapter 3**: Relative Motion Measurements. This chapter is concerned with answering the research questions Q2 and Q3. The chapter presents the proposed measurement system with a detailed model of the employed vision sensor. Additionally, the processes of creating synthetic data are outlined.
- **Chapter 4**: Modelling & Control Design. This chapter is concerned with answering the research questions Q4, Q5, and Q6. The chapter presents a background over the common vision-based control approaches, then the proposed control scheme is formulated. with the mathematical model of the Gangway system. Additionally, the different parameters of the MPC are discussed. and the design of the employed neural network for disturbance anticipation is outlined.

- **Chapter 5**: Results. This chapter evaluates the performance of the proposed solution for automating the docking procedure. The controller is first tested for the nominal case with multiple scenarios (i.e. with and without disturbance anticipation, different MPC settings). Then, tests are preformed against the plant model mismatch. Lastly, the performance is evaluated for a more extreme case in terms of the amplitude of the sea-induced motion.
- **Chapter 6**: Conclusions and Recommendations. This chapter discusses the project outcome and the potential space for enhancement and future work.

Chapter 2

System Architecture

This chapter introduces the Gangway system architecture as designed by Bosch. In terms of its mechanical structure, actuator, and measurement system. Furthermore, the physical limitation and control task requirements of the system are presented. Then, the current control loop is outlined with the operator function description.

2-1 Reference frames

The vessel, which the Gangway system is attached to, is subject to different disturbances (e.g., sea state, wind gust). The induced motion via sea state causes undesired motion at the Gangway tip.
As stated in Chapter 1, the problem of motion compensation can be recast as a relative motion tracking problem. Hence, instead of describing the Gangway system within a non-inertial frame, we can assume that the fixed-world frame of reference is attached to the Gangway base. This means that the offshore platform is moving and the Gangway base is fixed in the 3D space. Certainly, this hypothesis will simplify the system mathematical model and the control design.
Accordingly, we need to define a set of reference frames for the various rigid bodies in the system (i.e. the base, the offshore platform).
Figure 2-1, depicts the different reference frames for the Gangway system. Where Ψ_t represents the reference frame of the docking area on the offshore platform and Ψ_b is the reference frame of the Gangway base which is attached to the fixed-world coordinates as the aforementioned assumptions states. The reference frame Ψ_c represent the vision sensor coordinates. Note that the homogeneous transformation is fixed between the vision sensor frame Ψ_c and the Gangway tip reference frame Ψ_{tip} assuming the Gangway is a rigid body and no deformations occur.
Furthermore, three hydraulic actuators facilitate movement between the base reference frame Ψ_b and the tip reference frame Ψ_{tip}. The actuators form an open-chain kinematic with a three-DoF. The slewing and luffing actuators are rotational joints and lead to rotations in the

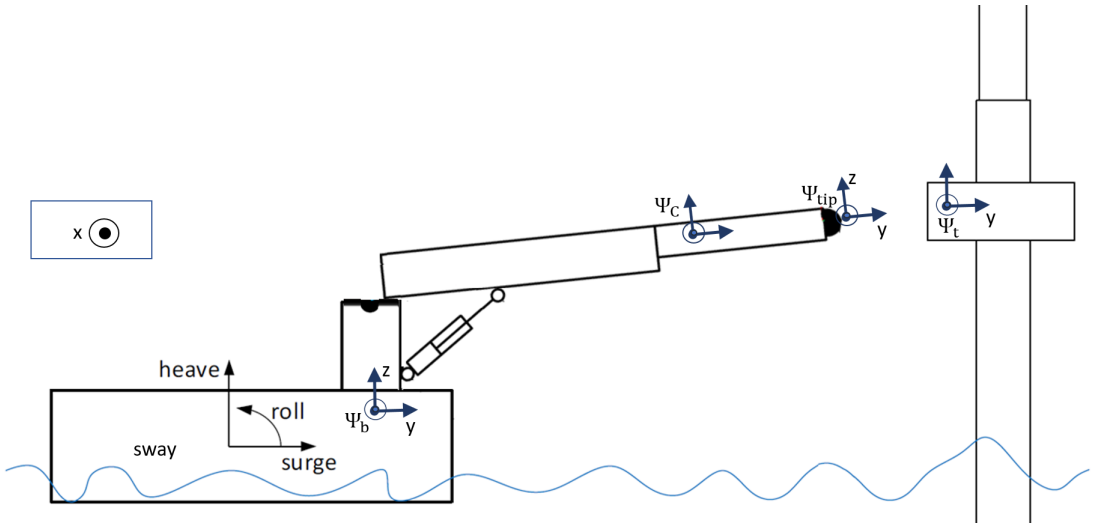

Figure 2-1: Definition of the relevant reference frames gangway model.

horizontal and vertical planes around yaw and pitch axes, respectively. The telescoping is a prismatic joint along the Sway axis, see Figure 1-3 for axes conventions.
This kinematics chain will be utilised within the Gangway mathematical model in the control design in Chapter 4. Where the joints displacement is represented by the state variable q_n with $q_n = [q_{slew}, q_{luff}, q_{tele}]^T$.
Figure 2-2 depicts the Gangway system workspace. This workspace represents the set of the reachable points by the Gangway tip in 3D space.

2-2 Mechanical structure

Besides some safety and redundant components, the system structure mainly consists of a rigid mechanical structure, actuators, and sensors.
For the structural design, the following was taken into account by Bosch during the design phase of the Gangway system:

- The lowest vertical eigenfrequency of the Gangway is designed to be at least 3Hz to avoid excitation by walking personnel (human walking excitation frequency is around 2Hz) [17].
- The Gangway is designed to be stiff to contribute to the safe feeling of personnel in transfer including load (e.g. equipment, cargo, etc). Both bending and torsional stiffness are considered.
- Hydraulic actuators were considered because of the high rigidity and high torques/forces these actuators can provide.

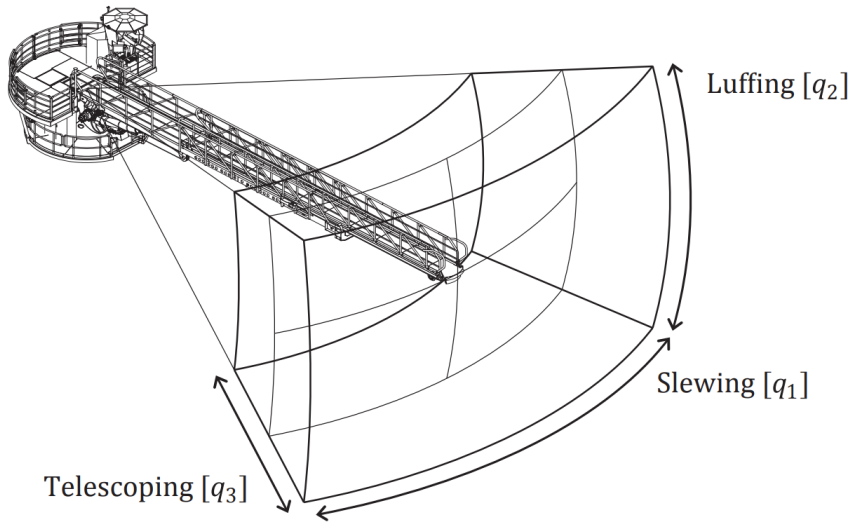

Figure 2-2: The workspace and Degrees of freedom in which the gangway operates. From [7].

2-3 Actuators

Each actuator is controlled by a specific Programmable Logic Controller (PLC) referred to as a Hydraulics-capable Numerical Control (HNC) computer. HNCs accept a position and a velocity setpoint. The HNC controls the voltage signals sent to the actuator valves.
Accordingly, the control on the joint-level control is already designed by Bosch and the High-level control is the main contribution in this project. In addition, Gangway's actuators are configured as follows.

- The slewing drive, to rotate the Gangway.
  The slewing actuator consists of two rotational drives working on a large slewing ring, as shown in Figure 2-3.

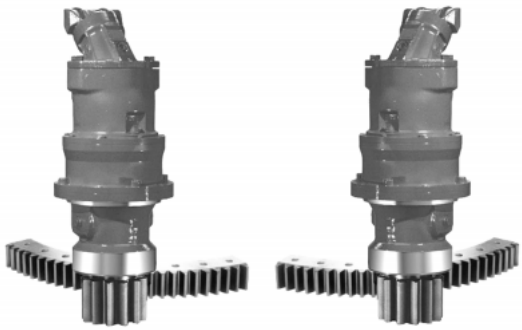

Figure 2-3: Two hydraulic rotational motors with gearbox and pinion acting on a slewing ring. From [7].

- The luffing cylinder, to raise and lower the gangway.
  For the luffing cylinder, a double driven cylinder is used. Which means that both

chambers in the cylinder are pressurised and connected to the valves. With the oil flow controlled to both chambers, double driven actuators can exert pushing and pulling forces on the environment. See Figure 2-4.

- The telescoping winch, to extend and retract the moving part of the gangway.
  The moving part is driven by a direct drive hydraulic motor. The motor drives a winch drum which connects to the moving part with a cable. See Figure 2-5 to the left: The telescope winch. The winch drum translates the rotational motion of the motor to a linear motion of the cable and the telescope. As shown to the right in Figure 2-5.

Relevant operational constraints are shown in Table 2-1 [5,6].

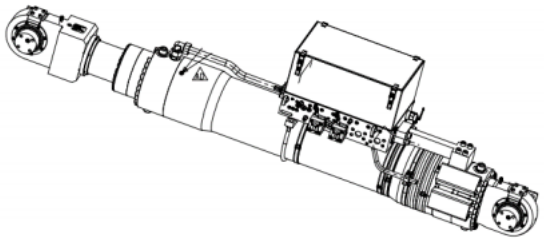

Figure 2-4: Luffing cylinder. From [7].

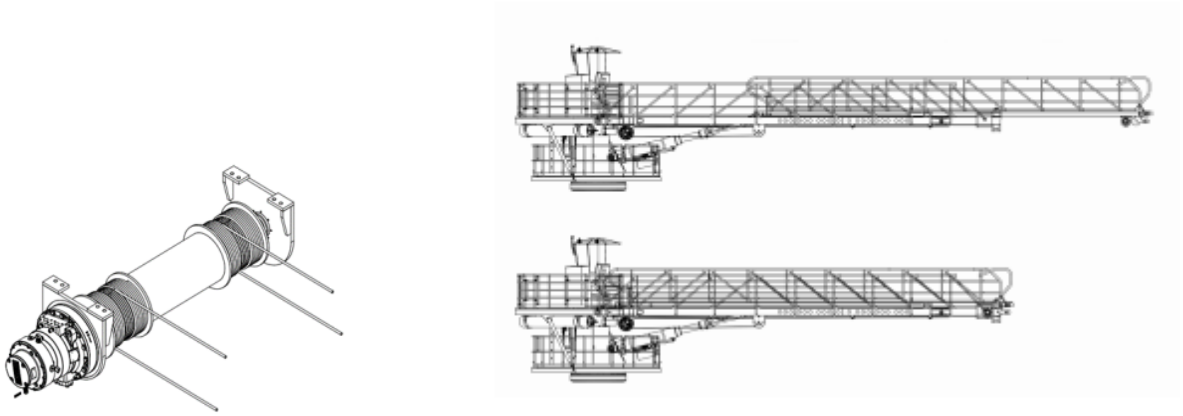

Figure 2-5: The telescope winch and the telescope extension using a cable system. From [5].

Table 2-1: The operational limits of the hydraulic actuators

	Slewing drive	Luffing cylinder	Telescoping winch
Work range	0 to 360 deg	-23 to 23 deg	17 to 27 m
Maximum operational speed	8 deg/s	0.13 m/s	1.6 m/s
Maximum operational force/torque	284 kNm	927 kN	27 kN

2-4 Disturbances

The primary source of disturbances which the Gangway system is predominately subject to is the vessel's induced motion via sea state.
It is stated in Chapter 1, the problem of motion compensation problem can be recast, through the relative motion hypothesis, as a dynamic target tracking (i.e. the offshore platform). Nevertheless, understanding the nature of the target motion (i.e. the vessel's induced motion) is still of great interest for prediction and control design as it will be further discussed in Chapter 3 and 4.
Regarding the sea state, an accurate approximation can be made by a representation of waves that consists of a spectrum of harmonic waves. Well-known spectra are the Pierson-Moskowitz and the JONSWAP spectra [18]. The latter is based on measurements carried out in the North Sea [19].
When the Dynamic Positioning (DP) system of the vessel is enabled (i.e. prior to docking the Gangway). The DP system actively controls the propellers, rudders, and thrusters so that the induced motion is attenuated on the horizontal plane. However, the measurements and control signals are not perfect. This results in small deviations (0.5 to 2 m), relatively to the size of the ship, along the surge and sway axes.
The response of the vessel to a wave spectrum is represented by a set of transfer functions along the principal axes. These transfer functions are known as Response Amplitude Operators (RAO). The RAOs contain a magnitude and phase response for the wave frequencies and angles from which the waves hit the vessel. Using the wave spectrum and the RAOs, vessel motions can be estimated [20]. However, RAOs are highly dependent on the vessel characteristics (i.e. shape, mass distribution).
This approach required accurate information about the vessel and its DP system characteristics. This is usually not accessible since most of the manufacturers are very conservative over sharing such information. Therefore, this approach is not considered in this project.
Alternatively, Bosch provided a data set for the vessel residual motion in DP mode while the Gangway is docked onto the offshore platform. In Chapter 4, this data set is utilised to train a neural network type NARX to anticipate the incoming disturbances in a multi-step-ahead fashion. Intuitively, the performance of the proposed control method benefits significantly from anticipating the external perturbation (the wave-induced motion).
Figure 2-6, depicts the vessel response to the sea state which results in sinusoidal motion on six axes that have the following characteristics:

- The wave period should not exceed 12 seconds and 4 seconds for the shortest wave period with a significant wave height H_{sig} no more than 3.0 m [6].
- Motion on roll, pitch and yaw axes deviate between ± 4 degrees and that is mainly due to the length and the huge mass of the vessel which can damp out the perturbations on the aforementioned axes.
- Maximum wind speed: 20 m/sec.

These three points define the operating window which the Gangway system is designed to function within. Furthermore, other external perturbations (e.g. walking personnel, moving cargo) have a less significant impact on the Gangway system are therefore out of the scope of this project.

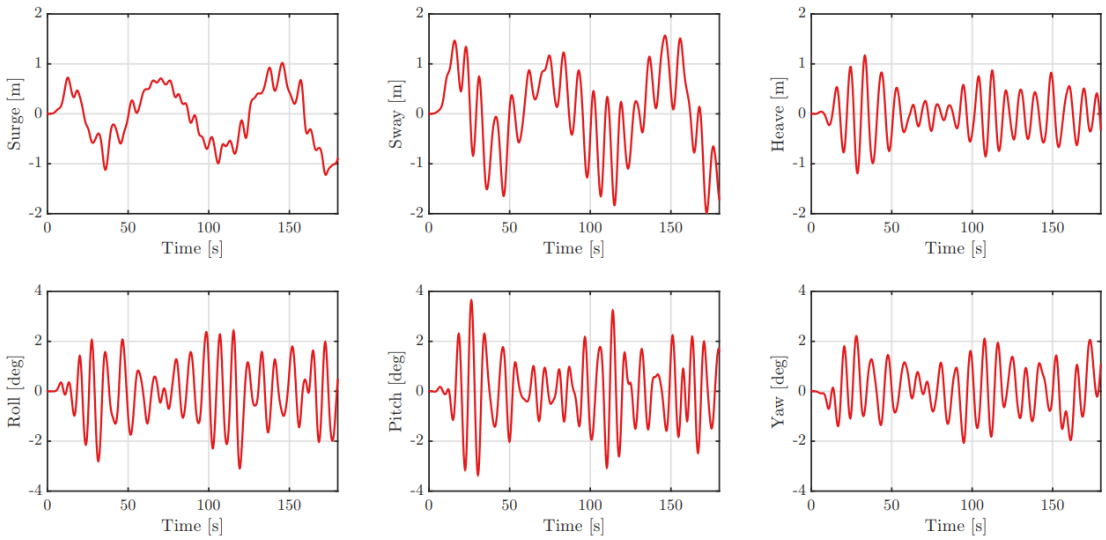

Figure 2-6: Ship movements in six degrees of freedom in a time window of three minutes.

2-5 Measurement system

The Gangway system consists of the following set of sensors.

2-5-1 Joint-level sensor

Position and pressure sensors on the joint-level to regulate the position and the hydraulic flow of the system actuators. These low-level control loops are realised with the HNCs.

2-5-2 Motion Reference Unit

The Gangway system counteracts the induced motion on the vessel by utilising a Motion Reference Unite (MRU). This sensing unit is capable of detecting the vessel motion in six Degree of Freedom (DoF). MRU is also referred to as an Inertial Measurement Unit (IMU). Where it utilises accelerometers and gyroscopes to measure its location and orientation. Usually, the MRUs manufacturers, employ a set of filtering and signal processing techniques within to provide good readings [21, 22]. However, due to the double integrator that is applied to the filtered MRU data, A small bias in the acceleration signal can result over time in a large position error.
Moreover, the Gangway system is employed with three MRUs at the Gangway base for accuracy and redundancy. Readings from these MRUs are averaged and considered as one MRU. Figure 2-1, the reference frame of the MRU is depicted in the base of the system Ψ_b.

2-5-3 Tip force Measurements

When the control task involves the robot interacting with the environment, a pure motion control scheme becomes insufficient to execute the manipulation task. Alternatively, a control

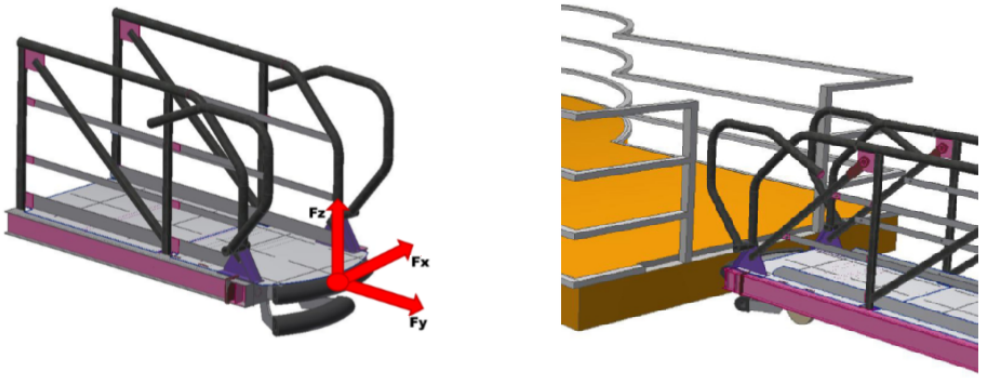

Figure 2-7: To the left, the definition of forces in the tip. To the right, the docking interface at an offshore wind turbine. From [5].

scheme with force/torque sensors can provide adequate haptic feedback to the robot.
In our case, to guarantee a safe connection with the offshore structure, the Gangway should exert a specific amount of force onto the docking area. Also, to avoid damaging the offshore platform, this exerted force should be actively regulated so that it does not exceed a certain limit.
Table 2-2 shows the required force and the force limits that the Gangway system can exert.
In order to measure the forces at a robot tip, force/torque sensors are placed precisely between the tip of the robot and the tool-point. In the Gangway system, three force sensors are placed along the principal axes at the end of the telescoping part behind a rubber bumper which was designed specifically to have a predetermined stiffness [6, 7], see Figure 2-7.
The contact force will be translated to the force sensors through the rubber bumper. When the bumper is in contact with the structure, the friction force helps to avoid stick-slip motion. The stiffness of the bumper will be used to model the force sensor in the simulation environment.

Table 2-2: Desired tip forces and acceptable forces along the tip principal axes [6], as depicted in Figure 2-7.

	Wind turbine monoplie [N]	Design force [N]	MCG Limit [N]
F_x	0 - 1000	4000	55000
F_y	4000 - 8000	20000	65000
F_z	0 - 1000	4000	45000

2-6 Control scheme and operator input

The low-level control of the Gangway system is realised via regulating the position and velocity of each hydraulic actuator separately with the HNCs. Where the operator uses three joysticks input to influence the velocity and positions setpoints of the actuators. The Gangway system with the actuators dynamics were considered to behave as three decoupled second-order sys-

tems with a bandwidth of $w_n = 6$ Hz and a damping ratio of $\zeta = 0.8$. This assumption was made by Bosch to substitute the plant dynamics with the aforementioned characteristics.
Moreover, as seen in Figure 1-5, the high-level control scheme of the Gangway system employs an MRU in a feedforward fashion to actively compensate for the induced motion.
The position control of the Gangway tip depends on the joints encoders and the MRUs to compensate for the induced motion.
In order to maintain the connection between the Gangway tip and the offshore platform, we cannot depend purely on position control due to the MRU drift error and a force control scheme becomes vital for maintaining contact with the offshore platform [7].
Accordingly, one-dimension force control loop is on parallel with the position control loop and the force control is enabled once the contact with offshore structure is initiated.
Bosch defines the control task requirements as:

- To guarantee safe passage and to avoid damaging the offshore platform. The contact force along the contact perpendicular axis should be within the limits as defined in Table 2-2.
- The time it takes the operator to perform the docking is 1 to 3 minutes which depends on his/her experience [7]. Thus, to increase the efficiency of the system, it is expected from the proposed system a shorter docking time.
- The current setpoint signals of the actuators is delivered via the joysticks in velocity and position terms. Hence, to match the compatibility with the employed HNC structure, the proposed control scheme should provide both velocity and position setpoints to the actuators.

2-7 Conclusion

This chapter outlined the Gangway system design and critical component of the control system as designed by Bosch. In addition, the current control approach is outlined with the control task requirements. With that, the first research question in Section 2-4 has been addressed. Based on that, a kinematic model of the Gangway is derived. Additionally, Bosch provides an approximation of the joint-level control loop of the Gangway system. This model is employed in the simulation environment and within the proposed control methods in Chapter 4.

Chapter 3

Relative Motion Measurements

This chapter is concerned with answering the key research questions:

- *How to measure the relative motion between the Gangway and the docking area?*
- *What kind of sensing technologies are included in the measurement system for the automated docking?*

3-1 The measurement system

Enabling the automated docking of the Gangway system can be translated into eliminating the human factors from the control loop. This is done by substituting the operator's function with a (high-level) control strategy that employs a suitable measurement system.
Correspondingly, as a starting point in this research, the preliminary choice for the proposed measurement system is based on the fact that the operator uses mainly his/her visual sensory information while steering the Gangway. Moreover, one cannot depend purely on MRU data for estimating the relative motion. This is mainly due to the drift error.The problem of mimicking the operator's perception can be recast as a relative motion estimation problem. Which is a common problem in robotics and well-studied in literature.
During the literature study phase of this project, various sensing technologies were initially considered and reviewed as classified in Figure 3-1. To choose a proper measurement system, the proposed measurement system should not only be able to estimate the relative motion but also to detect the location docking area on the offshore platform. This is possible by detecting the features of the target.
Mainly, there are two types of features; geometric (cylindrical, angle, etc.) and textural (fiducial marker, retroreflective tape, etc.). For example, in the space industry, a spacecraft docks onto the target, a process referred to as a space rendezvous. The spacecraft acquires information over the target pose and velocity in order to minimise the impact force. Using a cutting-edge vision system referred to as 3D Flash LiDAR Camera the relative motion is estimated by first capturing the geometrical and textural features of the target, [23, 24].

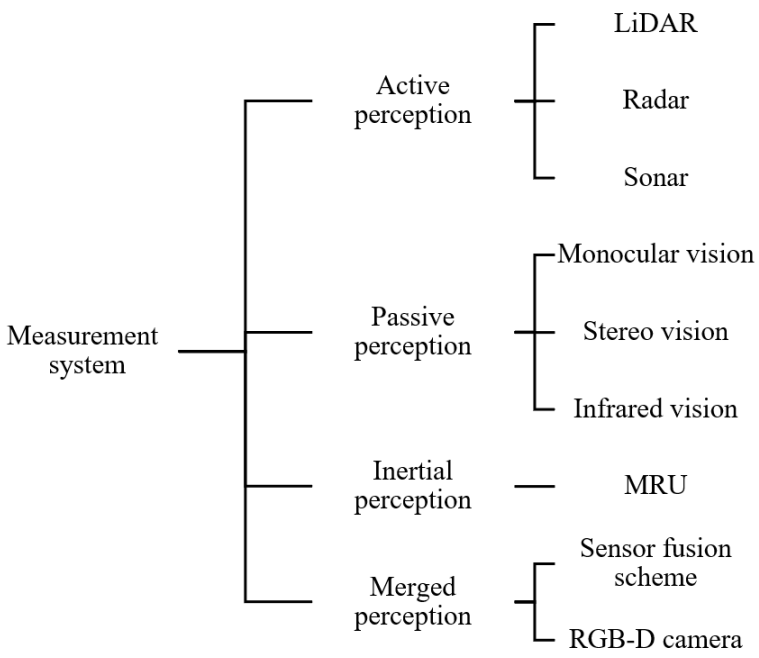

Figure 3-1: Classification of range sensing technologies

Similarly, to achieve the automated docking of the Gangway, the relative motion between the Gangway and the offshore structure should be estimated and the exact location of the docking area should be detected. So, it is a matter of tracking a dynamic target (i.e. the docking area) then docking onto the target. In [25–27], a robotic manipulator is employed to track and grasp free-flying objects in the 3D space while depending purely on a vision-based measurement system.
Correspondingly, the automated docking task has a strong point of resemblance to the process of grasping a flying object. Together with the aforementioned criteria, a vision-based measurement system would be a good fit for the application of automated docking.
However, for the force control task (i.e. regulating the contact force), as reported in Chapter 2 that; due to MRU drift error, tip force measurements are essential elements to maintain continuous contact and to avoid damaging the offshore structure.

3-2 Sensor architecture and sensor placement

In literature, there are various architectures of vision-based measurement systems. The most common ones namely are a monocular camera, a stereo camera, and multiple monocular cameras.
To maintain simplicity in system and control design, a monocular camera was chosen.
Mainly, there are two different configurations when it comes to placing a vision sensor within a robotic manipulator system; eye-in-hand or eye-to-hand. In the first configuration, the vision sensor(s) attached on the robot end- effector. Whereas in the second, the sensor(s) is fixed in the 3D space with a field of view focused on the workspace of the control task, see Figure 3-2.

From a control point of view, it can be classified as a collocated system or a non-collocated one, respectively. Additionally, for an object-tracking task, eye-in-hand is more appealing to ensure that the tracked features stay in the field of view [28]. Hence, this configuration is employed in the proposed control scheme in Chapter 4.

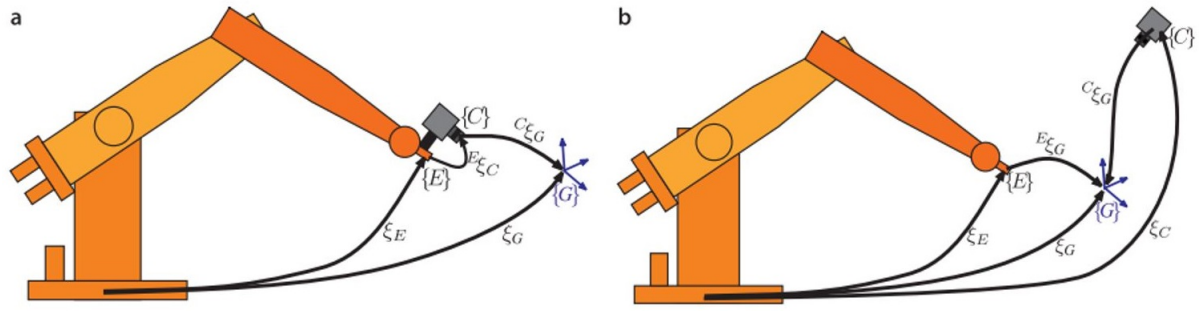

Figure 3-2: (a) eye-in-hand. (b) eye-to-hand. From [8].

3-3 Camera mathematical model

One advantage of employing a vision sensor in the measurement system is that a mathematical model can be defined. Hence, this analytic expression of a vision sensor can enable us to design and testing a vision-based control strategy in a simulation environment. This model is based on the so-called pin-hole camera model which employs the perspective projection (i.e. 3D to 2D mapping), see Figure 3-3. This model is widely employed in literature [9].
Hence, the function of this model is mapping the target coordinates from the Cartesian space into the image plane, which allow us to generate synthetic data. For a point P expressed in the world reference frame in 3D space, this mapping is realised through the following steps

1. Transforming the observed feature point P, represented in euclidean coordinates $P = [P_x, P_y, P_z]^T$, to homogeneous coordinates $\bar{P} = [P_x, P_y, P_z, \lambda]^T$, where λ is a scaling factor with default value $\lambda = 1$.

2. The homogeneous point $\bar{P}$ is, then, described in the camera reference frame via the homogeneous matrix H_0^c, which is the inverse transformation matrix between camera and the world reference frames H_c^0. This transformation results in the homogeneous matrix $H_{\bar{P}}^c$.

3. A 3D-to-2D mapping is, then, applied to the resulted homogeneous matrix $H_{\bar{P}}^c$.

4. The outcome of this process, a projected point $\bar{p} = [\bar{u}, \bar{v}, \bar{w}]^T$ represented in homogeneous coordinates.

5. The projected point can be retrieved to the euclidean image plane as $p = [\bar{u}/\bar{w}, \bar{v}/\bar{w}]^T$.

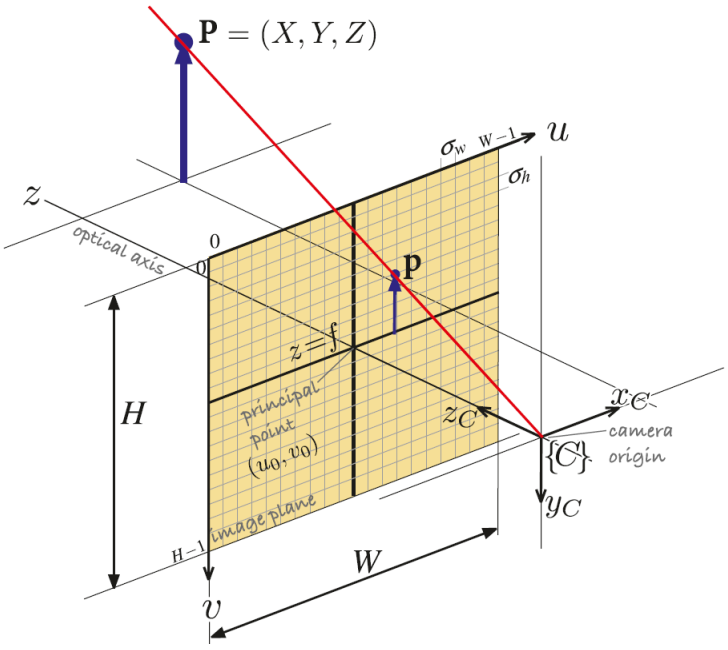

Figure 3-3: Perspective projection in the pin-hole camera model. From [8]

The corresponding mathematical formulation, of the aforementioned steps, is given as

$$\begin{bmatrix} \bar{u} \\ \bar{v} \\ \bar{w} \end{bmatrix} = \begin{bmatrix} f_x & 0 & u_0 \\ 0 & f_y & v_0 \\ 0 & 0 & 1 \end{bmatrix} \begin{bmatrix} H_0^c \end{bmatrix} \begin{bmatrix} P_x \\ P_y \\ P_z \\ 1 \end{bmatrix}, \tag{3-1}$$

with

$$H_0^c = \begin{bmatrix} H_c^0 \end{bmatrix}^{-1} = \begin{bmatrix} R_c^0 & t_c^0 \\ 0_{1\times 3} & 1 \end{bmatrix}^{-1}, \tag{3-2}$$

Here, f_x and f_y are the focal lengths on the horizontal and vertical axes respectively described in pixel units. The point $c = (u_0, v_0)$ is referred to as the principle point and ideally it is located in the centre of the image plane, Figure 3-3. These parameters are referred to as the intrinsic parameters.
The homogeneous matrix H_c^0 describes the transformation between the fixed-world reference frame and the camera reference frame. Accordingly, R_c^0, t_c^0 represent the rotational and the translational parts of H_c^0, respectively. This transformation matrix is known as the extrinsic parameters of the camera. Figure 3-4 depicts the transformation between the camera and the fixed-world reference frames.

The pin-hole camera model assumes an ideal thin lens, however, this is usually not the case. Commercial lenses distorts the light array prior reaching the vision sensor. The lens distortion mainly consists of radial and tangential distortion components and it can be modelled as an additive change to the projected point (x, y) in the image plane

$$\begin{aligned} x_{distorted} &= x\,(1 + k_1 r^2 + k_2 r^4 + k_3 r^6) \\ y_{distorted} &= y\,(1 + k_1 r^2 + k_2 r^4 + k_3 r^6), \end{aligned} \tag{3-3}$$

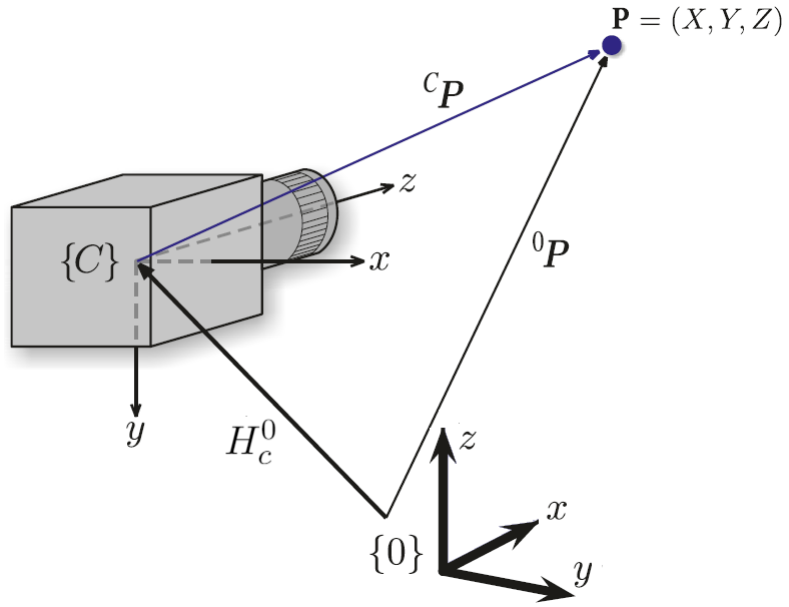

Figure 3-4: The transformation between target and camera reference frames. (Modified) From [8]

Figure 3-5: An image of a checkerboard captured with an ideal lens, a lens with positive distortion, and a lens with negative distortion, respectively. From [9].

with

$$r^2 = x^2 + y^2, \tag{3-4}$$

where k_1, k_2 and k_3 are the distortion coefficient. Figure 3-5 illustrates the different effect on the image when distortion exits with positive $(k_1, k_2, k_3 > 0)$ or negative $(k_1, k_2, k_3 < 0)$ coefficients. The process of estimating the camera intrinsic and extrinsic parameters and lens distortion is referred to as camera calibration.

3-4 Camera calibration

In order to simulate the camera model, camera parameters should be estimated. Calibration requires acquiring a set of images from different angles and various distances of a predefined planar object (e.g. a checkerboard), see Figure 3-6. Then, the observed features in the images

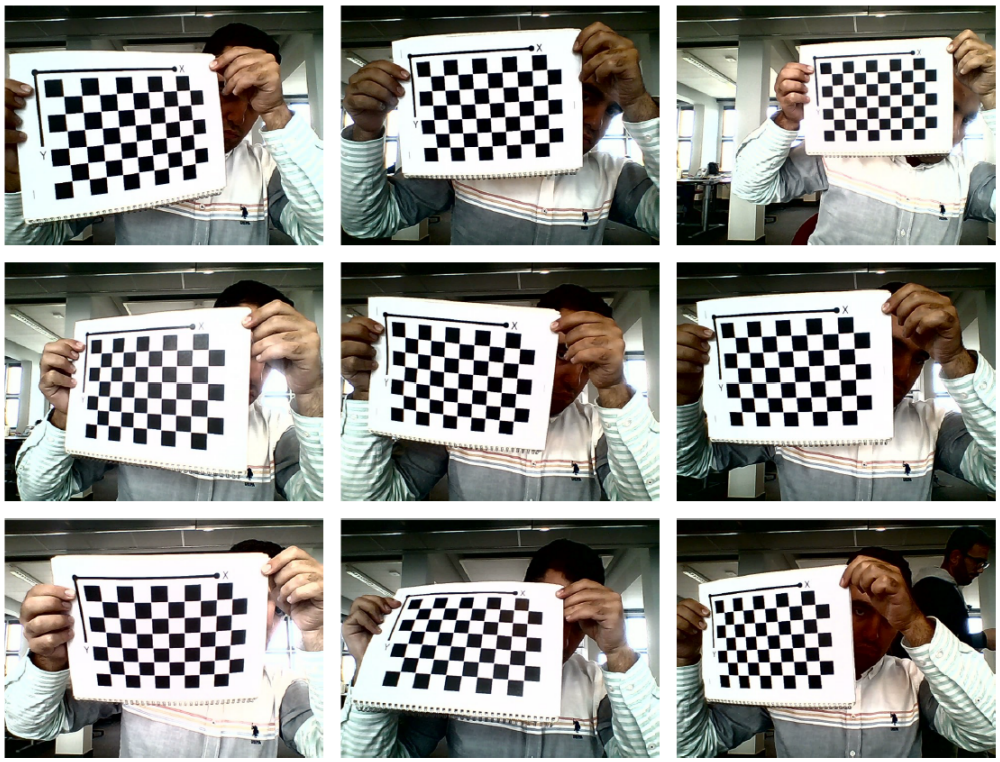

Figure 3-6: Captured images for camera calibration

of the checkerboard (i.e. corners and edges) are compared with the ground truth measurement of this planar object. Afterwards, the calibration problem is recast as a nonlinear least-squares optimisation problem for estimating the camera's intrinsic and extrinsic parameters [29, 30]. This procedure can be realised seamlessly in the Camera Calibration Toolbox for MATLAB. In robotics applications that involve a vision-based control scheme, only calibrating the vision sensor is often not sufficient. Therefore, additional calibration is required between the robot and the vision sensor. This is done by estimating the transformation matrices between the sensor(s) and robot reference frames either within an eye-in-hand or an eye-to-hand scheme [31].
Fortunately, the proposed control method in Chapter 4 solves the relative motion problem implicitly in the image plane. Where it has proven to be robust against various calibration errors and no on-site precise calibrations between the camera and the Gangway tip reference frames is required but rather a coarse measure will suffice.

3-5 Representing the offshore platform

Instead of detecting the docking area on the offshore platform, a solution is proposed to detect a fiducial marker the so-called Aruco marker, see Figure 3-7.
Hence, in the simulation environment, this target is considered to be the marker. Whereas, in reality, it can be attached next to the docking area. Aruco markers can be reliably detected and localised in both the Cartesian space and the image plane [32]. Therefore, Aruco markers

are widely employed in robotics and Augmented Reality (AR) as a source for the ground truth data in localisation applications.
From a critical point of view, One can argue that attaching a marker to each offshore platform sounds impractical. For example, over time, the marker surface might accumulate some dirt (i.e. dust, birds faeces), and the invisibility of the marker during the night and other bad weather conditions. This can cause a potential error in detecting the marker.
Some ideas were proposed during the literature study to tackle the aforementioned problems. For instance, employing a self-cleaning mechanism onto the marker stand and adding a NIR (Near Infra Red) illumination layer to the marker with a NIR camera on the Gangway, as proposed in [33].
On the other hand, the choice for this marker in this project is for the sake of simplicity and one can argue that, nowadays, many state-of-the-art algorithms are being developed in the area of object detection and localisation and the need to add visual marker to identify a specific object is not required anymore [34, 35].

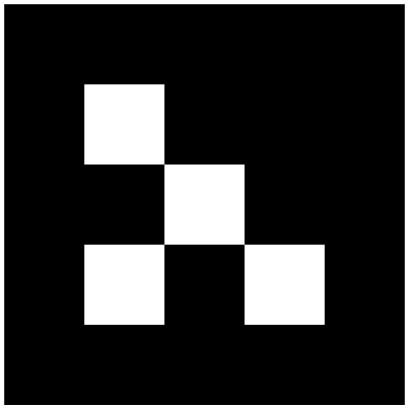

Figure 3-7: Aruco marker

3-6 Synthetic data

As stated above, the outcome of the literature study suggests a vision-based control scheme for solving the automated docking problem. However, there are no images recorded from the gangway tip. Therefore, synthetic data were made from the MRU data of a vessel with the Dynamic Positioning mode switched on. Figure 3-8 depicts the pipeline of generating the synthesised images.
First, to simulate a moving target, the MRU data is fed to the four dots to move in six-DoF. These dots represent the marker corners attached to the offshore platform. Then, the perspective projection model of the camera projects these dots to the image plane. After that, an image of the marker is wrapped into projected points. This process, also known as homography [8], is concerned in finding the transformation between two objects in a plane. Then, additive white Gaussian noise is applied to the generated image to make it more realistic. Finally, the image is passed to the marker detection script to detect the marker location in the image plane.

Figure 3-9 shows the target motion in 3D (MRU data) observed from the camera reference frame and the corresponding 2D mapping of this motion in the 2D image plane. Figure 3-10 is the 3D representation of the target relative pose to the camera that is attached at the tip of the Gangway.
Additionally, this scheme is embedded within the model-based control method in Chapter 4 to make use of the MRU data in predicting the target motion in the image plane in a multi-step-ahead prediction scheme.

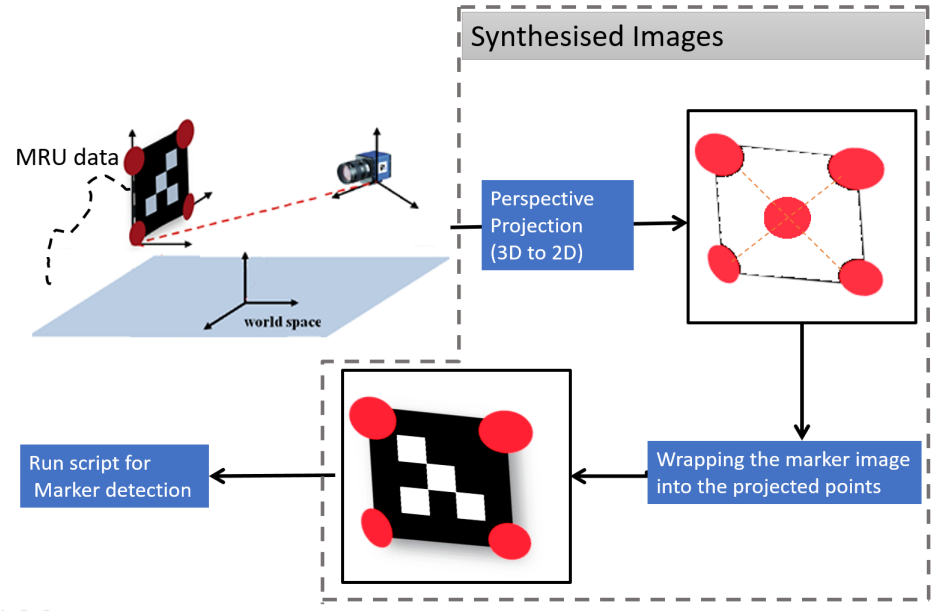

Figure 3-8: The process of generating the synthesised images

3-7 The motion model of the target

In Chapter 4, the proposed vision-based control method utilises the visual features explicitly in the control loop as an output to the system. In other words, the corners of the detected marker are considered to be the output signal of the measurement system.
In many control systems, the output signal is rather contaminated with noise and subject to disturbances. Likewise, the measurement of the detected location of the marker in the image plane should be corrected.
In the literature of dynamic object tracking, model-based tracking techniques are quite popular [31, 36–38]. The motion model of the object is not only utilised to estimate and correct the readily observed measurements, but it can also ensure the continuity of the output signal in case the object leaves the field of view, this is important to avoid instability in the control loop.
In [39], a survey is presented over the existing motion models and filtering techniques for dynamic object tracking. In [40], the so-called constant velocity model is employed with a linear Kalman filter as a state-observer to track a moving ship assuming the sea-induced ship motion is relatively slow.

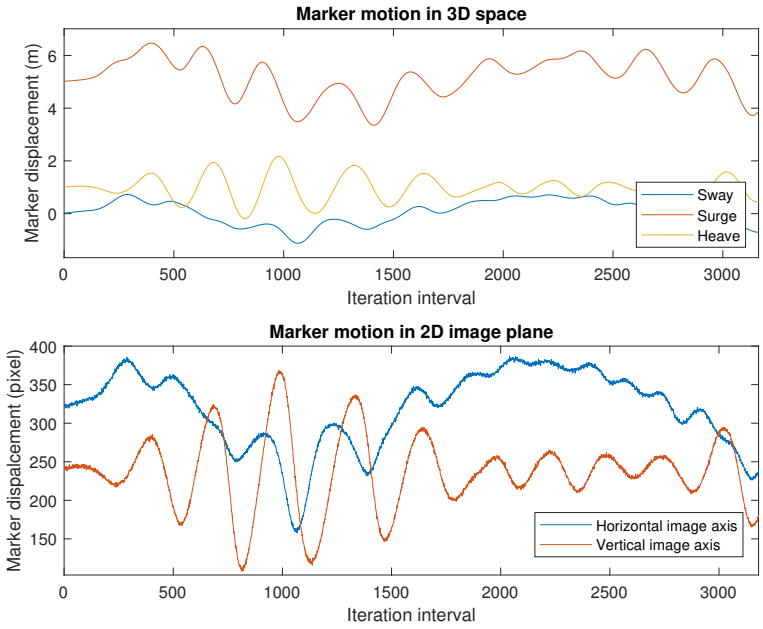

Figure 3-9: The target (the marker) movement is 3D observed from the camera reference frame and the corresponding 2D mapping in the image plane.

Similarly, in this project, the same approach was followed to track the moving marker. It consists of using a Kalman filter to estimate the corners and the centre of the marker.
This approach can also estimate, for a short time window, how the marker moves in the image plane when the detection is a not available anymore (i.e. when the marker leaves the field of view).
Figure 3-11 shows the real-time tracking data of the Aruco marker in the image plane, the images were taken from a standard web-cam with an update rate of 30fps. A sinusoidal-based motion that resembles the sea-induced motion was applied to the marker. Notice, when the marker leaves the field of view it becomes undetectable (for visualisation purpose the value filled with -1), Kalman filter still provides an estimate of how the target is moving. This estimation depends merely on the employed model and it is essential to avoid any discontinuity in the output signal which the tracking control depends on.
The so-called constant velocity model is the first order approximation of Taylor series, for a point $p = (p_x, p_y)$ in a 2D plane it can be given as

$$x(k) = A_{4x4}x(k-1), \tag{3-5}$$

with the state vector $x = [p_x, p_y, \dot{p_x}, \dot{p_y}]^T$ is the displacement and the velocity components of the horizontal and vertical axes respectively, and

$$A_{4x4}\begin{bmatrix} 1 & 0 & Ts & 0 \\ 0 & 1 & 0 & Ts \\ 0 & 0 & 1 & 0 \\ 0 & 0 & 0 & 1 \end{bmatrix}. \tag{3-6}$$

The marker is tracked by tracking the its centre and the four corners as an interest points. Hence,the previous model can be trivially extended to five point. The standard linear Kalman

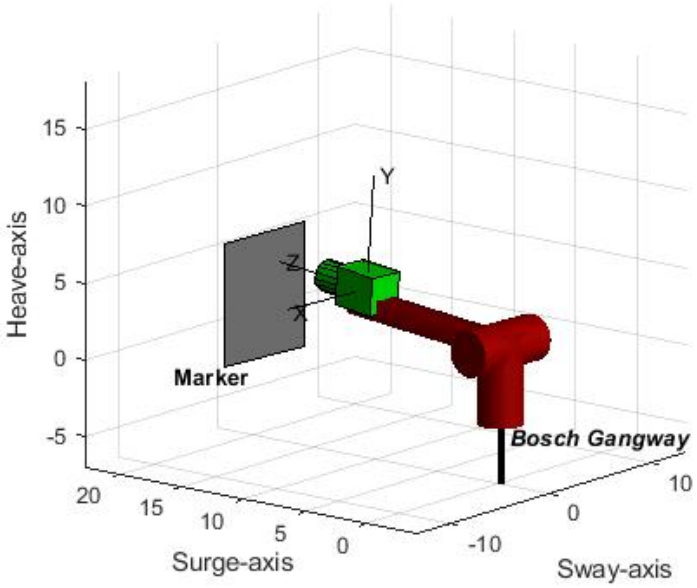

Figure 3-10: 3D representation of the a Gangway-like structure with the camera attached on the tip. The offshore platform is represented by the square grey marker.

filter is employed with the mathematical formulation that is given in [41].

3-8 Conclusion

A measurement system that is comprised of a monocular camera, MRU, and force sensors at the tip is required to enable the automated docking of the Gangway. Where eye-in-hand configuration (i.e. a camera is attached on the tip) is employed to ensure that the tracked features stay in the field of view. Next chapter presents the proposed control approach that accommodates this measurement system. Where, it was learned that vision sensor becomes insufficient for the force control task. Hence, a monocular camera alone cannot solve the docking problem and a multi-sensor solution is required.

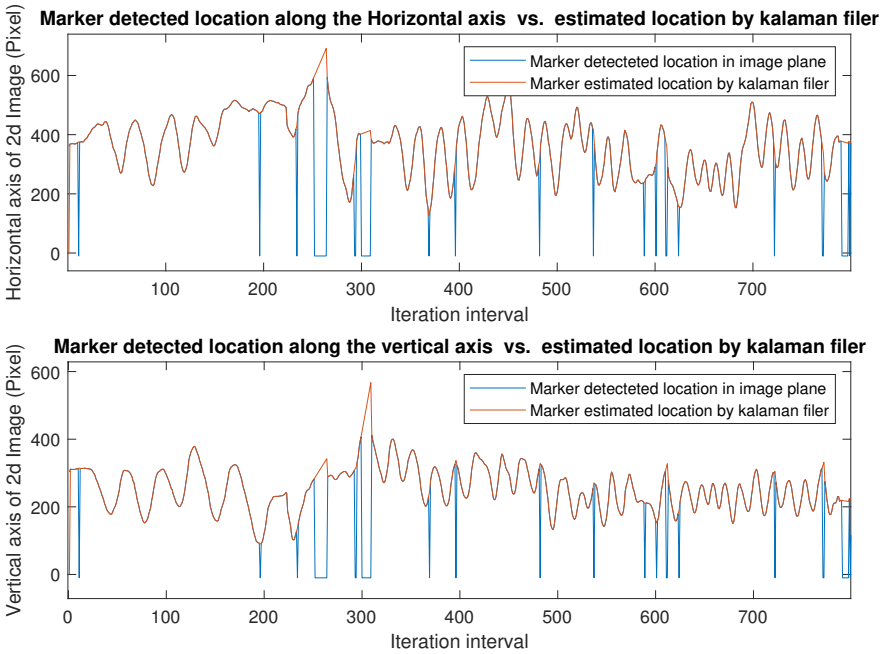

Figure 3-11: The process of generating the synthetic data

Chapter 4

Modelling & Control Design

This chapter is concerned with answering the key research questions:

- *How can a vision sensor be incorporated within the control loop for automated docking?*
- *Is there a control scheme that combines vision and force control while handling constraints?*
- *Is it possible to forecast the sea-induced motion? Would the proposed control method benefit from anticipating the external perturbation ahead?*

Thus, this chapter presents the modelling and control concept of the Gangway system. Where, first, a brief background over the vision-based control concept in robotics is given. Then, for the purpose of automated docking, a nonlinear Model Predictive Control (MPC) method is proposed. MPC is a model-based control approach, thus, a mathematical model of the Gangway system is derived. Subsequently, the MPC problem is formulated with a discussion over its parameters selection process. To enable the disturbance anticipatory property in MPC, a neural network with NARX topology is desired to forecast the sea-induced motion. Lastly, a brief analysis of closed-loop stability for MPC is shown.

4-1 The concept of vision-based control

In Chapter 3, it was concluded that a vision-based measurement system fits best for the relative motion estimation between the Gangway and the offshore structure. As a result, a measurement system with a vision sensor (i.e. monocular camera) will be employed in the control loop.
In robotics, integrating a vision sensor into the control loop is often described in the relevant literature in two different fashions: either in the open-loop [31, 33, 42] or closed-loop [43–45]. The former employs the term 'Look-and-move' which basically means the vision sensor gives the setpoint to the system each iteration without incorporating the visual feedback within

the control loop. The latter, also referred to as 'Visual Servoing', employs the vision sensor into the control loop as a feedback signal [46].
Usually, vision-based measurement systems have a relatively low bandwidth compared to the joint encoders of a robotic manipulator, and that is mainly due to the latency in image acquisition and processing [8]. Therefore, when it comes to employing a vision sensor within a control loop, it is reasonable to consider the control system of a robotic manipulator with a vision sensor as two cascaded loops; an inner loop for joint velocity control using the encoders feedback, and an outer loop that incorporates the visual feedback within the high-level control strategy, where the nature of the reference signal is chosen based on of the employed visual servoing approach, as seen in Figure 4-1.

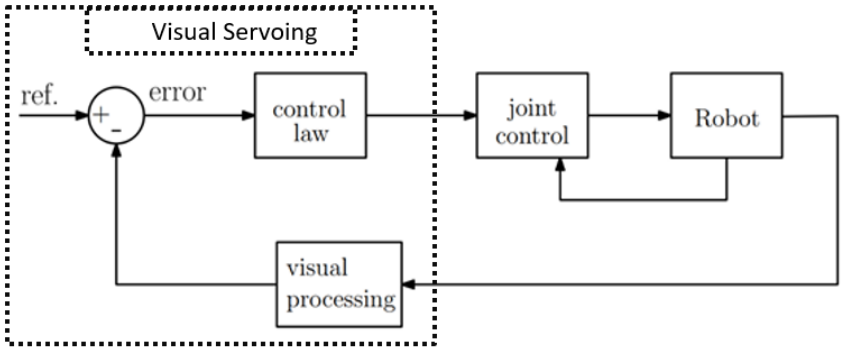

Figure 4-1: The general control scheme of visual servoing. (Modified) From [10]

Moreover, the mathematical formulation of a classical visual servoing scheme is given as

$$e(t) = s(t) - s(t)^*, \tag{4-1}$$

where $s^*(t)$ is the desired setpoint which its nature follows the same as $s(t)$ and usually is chosen as a constant [47]. For the sake of simplicity, we choose $s^*\ast$ as constant. s, one the other hand, can consist of a set of features that are readily available in the image data (image-based), or it consists of a set of three-DoF or six-DoF parameters, which must be estimated from image measurements (pose-based). In both cases, $s(t)$ can be related to the six-DoF velocity twist of the vision sensor by

$$\dot{s} = L_s V_c, \tag{4-2}$$

where V_c represents the spatial twist of the camera, and the so-called interaction matrix L_s, also known as the image Jacobian matrix, is the matrix which maps the velocity vector of the feature to the velocity of the camera. The image Jacobian is either an explicit or an implicit function of the target pose in 3D space depending on the employed VS concept pose-based or image-based, respectively.
The output of the visual seroving control is basically the desired spatial velocity of the camera. From the previous relationship

$$V_c = L_s^{\dagger}\dot{s}, \tag{4-3}$$

where the pseudo inverse, denoted by †, is usually employed here to avoid inverting an ill-conditioned Jacobian [47]. With a constant reference signal s^*, the previous relationship can be written in terms of $\dot{e}$

$$V_c = L_s^{\dagger}\dot{e}. \tag{4-4}$$

Since it is desired to have an exponential decrease of the error signal, we write

$$\dot{e} = -\lambda e. \tag{4-5}$$

Then, the final expression becomes

$$V_c = -\lambda L_s^{\dagger} e. \tag{4-6}$$

In case of a monocular camera attached at end-effector of a robotic manipulator, the desired special velocity of the camera can be translated into the desired joints velocity of the robot $\dot{q}$ with the robot Jacobian Jr

$$\dot{q} = -\lambda J_r^{\dagger} L_s^{\dagger} e. \tag{4-7}$$

One of the main challenges in visual seroving schemes is acquiring a full rank well-conditioned interaction matrix. Additionally, there are different schemes of visual servoing to design the interaction matrix L_s and the nature of the observed feature s. Where L_s can be an explicit function of the target pose in 3D space with respect to the camera in case of Pose-Based Visual Seroving (PBVS). Alternatively, L_s can be an implicit function of the target pose in case of Image-Based Visual Seroving (IBVS). Where it depends on the target measured features $s(t)$ and the camera intrinsic and extrinsic parameters.
The advantages and drawbacks of the different common schemes of visual servoing are discussed in the following subsections.

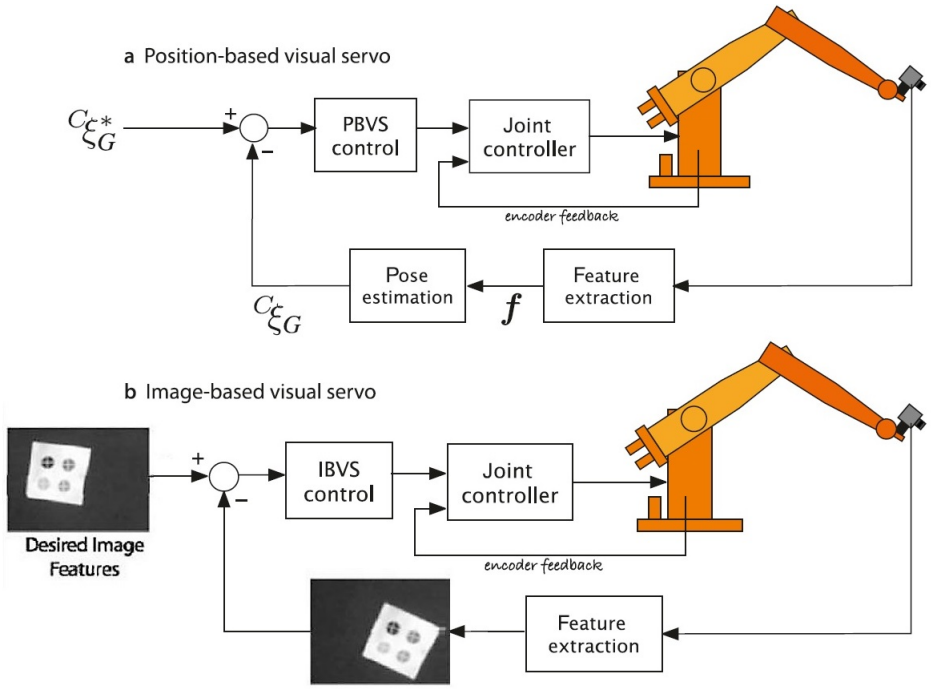

Figure 4-2: The different visual servoing schemes. (a) PBVS general control scheme the setpoint signal is the desired relative pose between the tip and the target. (b) IBVS general control scheme where the setpoint is the desired field of view of the target in the image plane, this solve the pose estimation problem implicitly when the tracking error converges to zero. From [8].

4-1-1 Pose-Based Visual Servoing (PBVS)

In the PBVS scheme, the control task is achieved within the 3D Cartesian space. This is achieved by estimating the relative pose between the target and the vision sensor. The reference signal here is given in Cartesian space where the error signal holds information about the current pose of the camera with respect to the target. This is realised using photogrammetry and sensor fusion techniques [48, 49]. Figure 4-2 depicts the general control scheme where the setpoint signal is the desired relative pose between the tip and the target. PBVS usually required multiple vision sensors (e.g. stereo camera) with precise calibration. Also, the relative pose estimation process is highly dependent on the accuracy of the camera's intrinsic and extrinsic parameters. This sensitivity might lead to a 'bad' convergence in the closed-loop. However, if the pose estimation is flawlessly attained and the camera is well calibrated then global asymptotic stability of the closed-loop system can be ensured.
Moreover, in the PBVS scheme, the robot end effector might leave the field of view which might result in a discontinuity in the measurement signal [8, 47]. This is considered a major drawback because this might results in discontinuation in the output signal which might lead the controller to unstable behaviour.

4-1-2 Image-Based Visual Servoing (IBVS)

Unlike the PBVS scheme, in IBVS, the task function represents the error in the 2D image space, as seen in Figure 4-2. Basically, the feedback signal here is the readily available location of the tracked features in the image plane, and the setpoint represents the desired location for these features in the image plane [8, 47]. With this, the relative pose problem is solved implicitly without the needs for multiple vision sensors nor for an excessive calibration of the vision sensor(s) parameters.
IBVS relies on basic image processing techniques and requires a minimum of three observed features to ensure well-condition image jacobian [47]. Therefore, IBVS is more computationally efficient and more immune to calibration error and noise [50]. Furthermore, in IBVS the observed features are kept in the field of view. However, due to the nature of the feedback signal, the 3D Cartesian trajectory is not considered. This might lead the robot to a singularity configuration (e.g. joint limits) [47].
Moreover, when it comes to stability analysis, IBVS can only ensure local asymptotic stability of the closed-loop and it might be attracted to a local minimum when the desired locations of the observed features are somewhat distant from the current locations [8, 47].

4-1-3 Visual Predictive Control (VPC)

IBVS proved to achieve adequate and robust performance against the camera and robot calibration errors and image measurement errors while assuring local asymptotic stability [51]. Nevertheless, classical IBVS schemes cannot deal with constraints such as joint limits and the camera field of view.
Visual Predictive Control (VPC) was first reported and formulated in the work of Allibert *et al* [11]. This control method considers the so-called Internal Model Control (IMC) structure. The process block contains the robotic system and the camera, as seen in Figure 4-3. The input U is the robotic control variable and the output s is the current value of the visual

features. For IBVS, the reference s^* is expressed in the 2D image plane, as the visual features, and can be static or dynamic [52].
The scheme of VPC offers not only constraints handling but also modelling and calibrations errors if the utilised internal model in the IMC block is the nominal model of the plant. This model can be acquired based on the image Jacobean matrix which can suffer from singularity condition (as it is the case with classical IBVS), [47].

4-2 The proposed control scheme

To enable the automated docking in a hierarchical fashion, the control task, during the design phase of this project, was categorised into two main parts; tracking the target (i.e. the offshore platform) and docking into the target.
This method is based on the standard nonlinear Model Predictive Control (MPC). Figure 4-4, depicts a high-level control scheme of the proposed method. This proposed scheme highly mainly resembles the general control scheme of VPC in the work of Allibert *et al* [11], see Figure 4-3. In a sense that, both are MPC-based approaches and in the nature of the reference (desired field of view) and the output signal of the target (target's features in the image plane). Similarly to the VPC scheme, the proposed method can handle the different constraints of the Gangway system such as workspace constraints, field of view constraints, and contact force constraints, see Table 2-1 and 2-2. However, the proposed scheme differs from the VPC scheme in numerous aspects. The following points highlight the main differences between the proposed scheme and the VPC scheme.

- **Different plant model considerations**
  In the VPC scheme in [11], the plant model is merely a free-flying camera that can move in six-DoF in the Cartesian space. Each DoF axis is represented by an integrator which means instant convergence to the setpoint. Clearly, this is highly abstract and simplified settings for a visual servoing problem. On the other hand, the derived model of the Gangway system is more concrete in describing realistic settings, more details in Section 4-3.

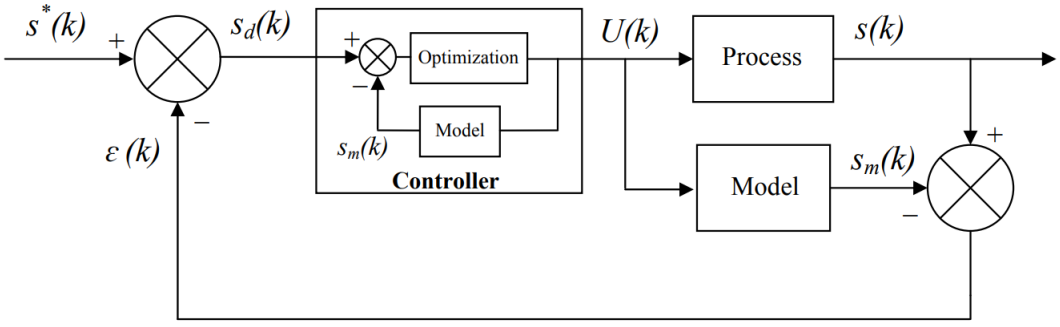

Figure 4-3: The general control scheme of VPC. This scheme, similarly to IBVS, takes the desired field of view as a setpoint $s^*(k)$. The Model block is the nominal model that is utilised in the internal model control structure. From [11]

- **No need for the IMC structure**
  In [11], it is stated that the internal model structure in the VPC scheme offers robustness against parametric uncertainties. The main function of this scheme is basically measuring the difference between the output of the real plant and the nominal plant model and adjusting the setpoint signal accordingly to compensate for the model mismatch. However, in reality, the image plane is discretised in pixels unit and the resolution of the image plane is rather insufficient to for minor setpoint adjustments which are needed in the case of occurring model mismatch while the target is close to the camera in 3D space (i.e. when the Gangway tip is in contact with the platform). Accordingly, during the extermination phase, the proposed control method showed robustness against different model mismatch cases (e.g. camera calibration, actuators dynamics). Thus, from a practical point of view, there is no need here for the internal model structure.

- **No need for the image Jacobian**
  In VPC and other visual seroving schemes, the image Jacobian matrix is employed in the model. However, the proposed method depends on the pinhole perspective projection model, as described in (3-1). Generally, it is difficult to ensure a well-conditioned image Jacobian. This is an inadmissible property, especially, when the camera has restricted movement, in case the camera is attached to a three-DoF structure (e.g. the Gangway system) instead of a six-DoF one (e.g. free-flying camera). In addition, the pinhole model maps the displacement of the target in 3D space to the 2D image plane rather than mapping the spatial velocity of the target as the image Jacobian do. For the case of automated docking, this is permissible since the target moves in sinusoidal-based motion (the sea-induced motion) with a slow velocity with a period of 4 to 12 sec. Hence, the proposed control method eliminates this potential source of singularities caused by an ill-conditioned Jacobian matrix.

- **Continuity of the measurement signal**
  In case of a sudden cluttering or invisibility of the target, the proposed can ensure the continuity of the target visual signal by employing the Kalman filter scheme described in 3-7. The Kalman filter estimates the target location in the field of view in case of sudden invisibility.

- **Different control task objectives**
  Although, both the proposed scheme and the VPC scheme are concerned with matching the current field of view with the desired one. However, to enable the automated docking of the Gangway system, regulating the contact force at the tip is essential to maintain a motionless contact while tracking the target motion. To effectively keep the contact force within the allowed limits, the proposed scheme also utilises the MRU measurements, more details in Section 5-1-2. Thus, from a control point of view, the proposed control scheme is concerned with a more challenging problem while comprises a more complex measurement system than the one the VPC scheme in [11].

4-3 Modelling considerations

Normally, standard nonlinear MPC is a model-based method. Hence, for the purpose of control design and simulation, a mathematical model that describes the Gangway system

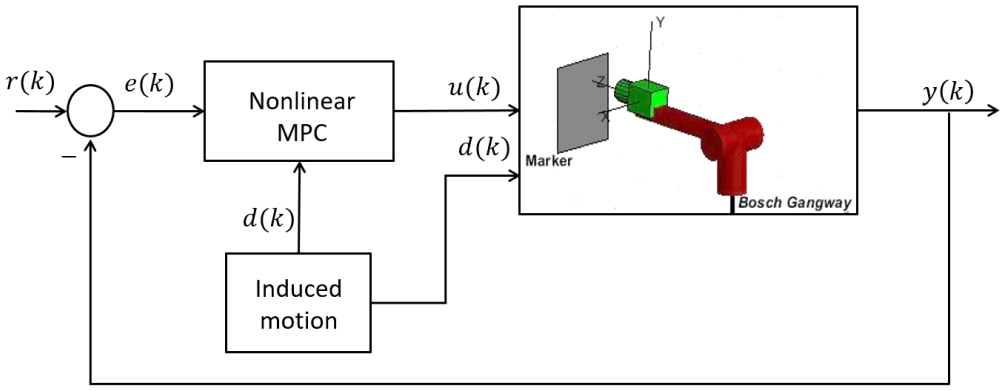

Figure 4-4: High-level control scheme of the proposed method.

with its measurement system should be derived.

4-3-1 Kinematics modelling

As stated in Section 4-1, due to the latency in image acquisition, and processing the visual servo control scheme is usually designed on a top of a low-level control which is employed on the joints level. Additionally, in Chapter 2, it is stated that each hydraulic actuator in the Gangway system is supplied with a position feedback loop, feedforward velocity control, and pressure feedback control. Based on that, Bosch suggests that the current closed-loop Gangway system with joint-level control is considered to behave as three decoupled second-order systems. This assumption was made by Bosch in order to substitute the low-level control loop dynamics of the Gangway system with the linear system as follows

$$G(s) = \begin{bmatrix} g(s) & 0 & 0 \\ 0 & g(s) & 0 \\ 0 & 0 & g(s) \end{bmatrix}, \tag{4-8}$$

where $g(s)$ is a second-order transfer function which is an approximation of the dynamics behaviour of the low-level control loop along each actuated joint with a bandwidth of $w_n = 6$ Hz and a damping ratio of $\zeta = 0.8$. Hence, $g(s)$ can be written as

$$g(s) = \frac{w_n^2}{s^2 + 2\zeta w_n s + w_n^2} = \frac{1421.29}{s^2 + 60.32s + 1421.29}\,. \tag{4-9}$$

The nonlinear MPC requires the derived model in a state space representation. Thus, the state space realisation of the subsystem $g(s)$ can be written as

$$\begin{aligned} \dot{x}(t) &= \begin{bmatrix} -60.32 & -1421.29 \\ 1 & 0 \end{bmatrix} x(t) + \begin{bmatrix} 1421.29 \\ 0 \end{bmatrix} u(t) \\ y(t) &= \begin{bmatrix} 0 & 1 \end{bmatrix} x(t) \end{aligned} \tag{4-10}$$

where $x(t)$ is the state variables vector of the closed-loop actuator dynamics(e.g. slewing). $u(t)$ is the setpoint signal of the actuator, and y is the corresponding actuator response.

Correspondingly, the state space realisation of the low-level Gangway system $G(s)$ is denoted by G_{ss}. Which takes the actuators setpoint as inputs variables and the responses of the actuators as output variables.
Accordingly, the open-chain kinematics model of the Gangway system was derived in an inertial reference frame assuming that, as stated in Chapter 1, it is a matter of relative motion. Hence, the Gangway base is attached to the fixed-world reference frame and the offshore platform is moving, see Appendix 1 for more details on the kinematics model. Figure 4-5, depicts a 3D visualisation the of open-chain kinematics of a Gangway-like mechanism (RRP) with two revolute joints (i.e. slewing and luffing joints), and one prismatic joint (i.e. the telescoping joint).

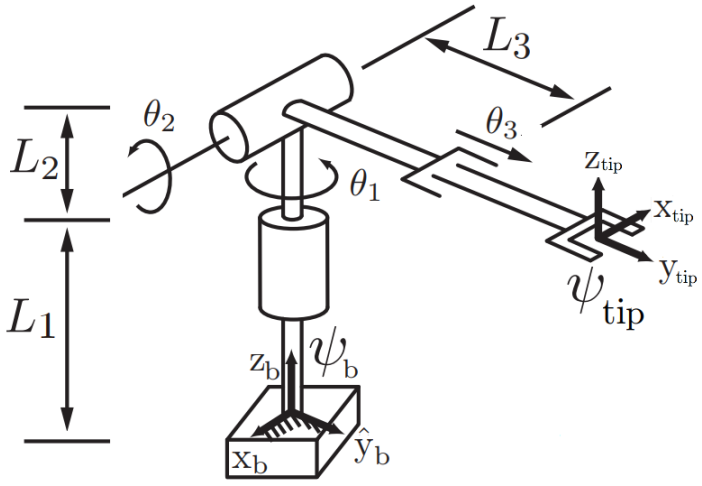

Figure 4-5: The 3D visualisation of the Gangway kinematic model. (Modified) From [12]. Where θ_1, θ_2, and θ_3 are the Gangway system actuated joints represented by slewing, luffing, and telescoping actuators, respectively. ψ_b and ψ_{tip} are the reference frame of the Gangway base and the tip, respectively. L_1, L_2, and L_3 are the constant displacements of the corresponding joints.

4-3-2 Incorporating the vision sensor within the model

This derived model should also incorporate a model for the vision sensor that is attached on the Gangway tip as Chapter 3 concludes. Now, despite the fact that visual servoing schemes usually employ the image Jacobian as the mapping matrix between the target spatial velocity and the corresponding velocity vector in the 2D image plane. Instead, the pinhole camera mathematical model, as described in (3-1), is employed for the following reasons:

- In visual servoing schemes, it is assumed that the vision sensor has six-DoF, whereas, in our case, the camera attached on the Gangway tip which has only three-DoF.
- Generally, it is difficult to ensure a well-conditioned image Jacobian, especially, with the restricted movement of the camera (three-DoF instead of six-DoF).

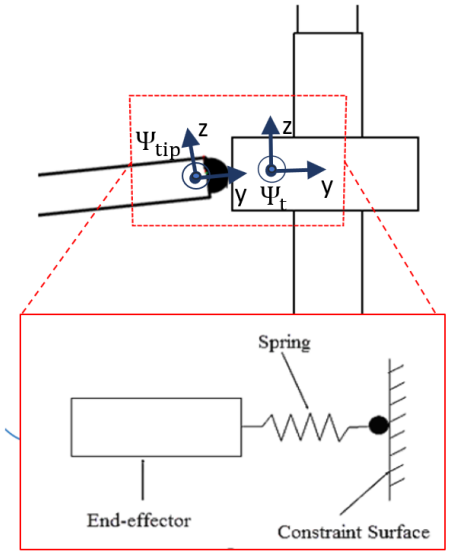

Figure 4-6: The mass-spring analogy of the contact force model.

- The pinhole camera model, reported in Chapter 3, describes the 3D-to-2D mapping in terms of displacement. This is convenient in the application of automated docking since the target moves slowly in the image plane with a period between 4 to 12 sec, which is originally the period of the wave-induced motion, as described in Section 2-4.

4-3-3 Force modelling

The contact force measurement is a vital element for the docking control task, thus, the derived model should include the contact force model.
Usually, in robotic manipulator systems, force control is combined with motion control [10]. When it comes to any manipulation process (e.g. docking onto a dynamic target), combining the feedback of vision and force sensors becomes essential in order to fulfil the control task requirements.
When the Gangway tip is in contact with the offshore platform, the contact force can be modelled as a mass-spring system as depicted in Figure 4-6 and shown in the expression below

$$f_c = K_b \ (y_{tip} - y_{platform}). \tag{4-11}$$

Here, K_b is the stiffness of the bumper at the tip of the Gangway. A few tests were carried out by Bosch, to identify the bumper stiffness, show that the bumper stiffness behaves linearly in the operating range [6]. The term $(y_{tip} - y_{platform})$ is the difference between the Gangway tip and the offshore platform along the perpendicular axis respectively.
Ideally, the force feedback is only enabled when the robot is in direct contact with the target/environment, hence to ensure that $f_c \geq 0$ in the derived model, the following applies

$$f_c = \max(0, K_b \ (y_{tip} - y_{platform})). \tag{4-12}$$

4-3-4 The nonlinear state space model

During the design phase of the proposed control method, it was noticed that in order to fulfil the force control task requirements, the target 3D motion should be incorporated within the derived model, more details in Section 5-1-2.
Now, considering the aforementioned assumption with the Gangway is fixed and the target is moving, and given that in the real system the MRU can provide the spatial velocity measurements of Gangway base, the nonlinear model is extended to include the MRU readings as external perturbations that can be mapped into the target spatial motion.
Consequently, the continuous-time nonlinear state space representation of the Gangway with the measurement system can be given as follows

$$\begin{aligned} \dot{x}(t) &= f(x(t), u(t), d(t)) \\ y(t) &= h(x(t)) \ . \end{aligned} \tag{4-13}$$

Here, the state vector $x(t)$ represents the Gangway joints displacement, and the target position in 3D space, respectively. The input vector $u(t)$ is the tip/camera spatial 3D velocity, and the sea-induced spatial velocity $d(t)$ acts as external perturbations to the system. The output vector y is the marker readily observed features coordinates in the 2D image plane (four corners and the centre of the marker), and the contact force response along the perpendicular axis with target, respectively.
Moreover, the nonlinear state transition function $f(x, u)$ is merely the inverse Gangway Jacobian matrix $J^{-1}(x)$ and the mapping matrix $Ad_{H_{target}^{MRU}}$ between the external perturbation and the target spatial velocity, respectively. Lastly, the output function $h(x)$ is the perspective 3D-to-2D projection pinhole camera model, as described in (3-1). This results in the target's detected features $p_{x,y}$ (marker's centre and corners). The second part of $h(x)$ is the contact force model along the contact perpendicular axis.
A more detailed description of the aforementioned variables and function is given below

$$\begin{cases} x & = [q_n, q_g, P_{target}]^T; \ \ x \in \mathbb{X} \subseteq \mathbb{R}^{12} \\ q_n & = [q_{slew}, q_{luff}, q_{tele}]^T \\ q_g & = G_{ss} \ q_n \\ P_{target} & = [P_x, P_y, P_z]^T \\ u & = [Tip_{vel}]; \ \ u \in \mathbb{U} \subseteq \mathbb{R}^3 \\ Tip_{vel} & = [\dot{x}_{tip}, \dot{y}_{tip}, \dot{z}_{tip}] \\ d & = [vessel_{vel}]; \ \ d \in \mathbb{D} \subseteq \mathbb{R}^3 \\ vessel_{vel} & = [surge_{vel}, sway_{vel}, heave_{vel}] \\ y & = [image, force_y]^T; \ \ y \in \mathbb{Y} \subseteq \mathbb{R}^{11} \\ image & = vec(p_{x,y}); \ \ p_{x,y} \in \mathbb{P} \subseteq \mathbb{N}^{2\times 5} \end{cases} , \tag{4-14}$$

with

$$\begin{cases} f(x,u,d) &= \begin{bmatrix} G_{ss}\ x(t) \\ J^{-1}(x(t))\ u(t) \\ Ad_{H^{MRU}_{target}}\ d(t) \end{bmatrix} \\ h(x(t)) &= \begin{bmatrix} Pinhole(x(t)) \\ f_c(x(t)) \end{bmatrix} \end{cases}. \tag{4-15}$$

Note that, q_g here is the joints displacement response of the low-level dynamics G_{ss}, described in (4-8) and (4-10), and q_n is the joints displacement setpoint for the low-level control loop. Accordingly, the open-loop block diagram that describes this model is depicted in Figure 4-7.

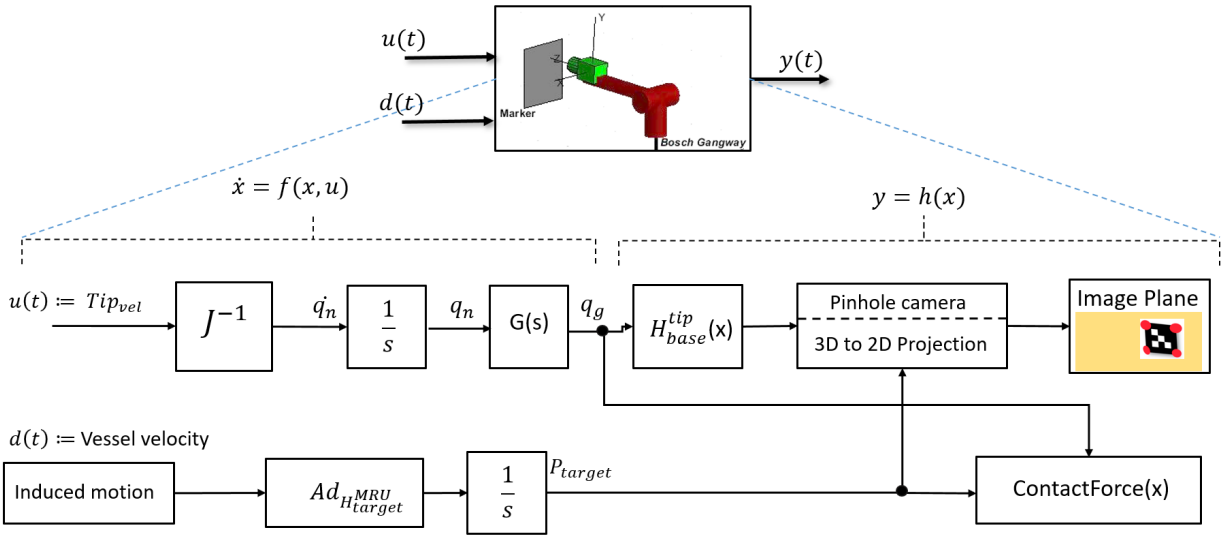

Figure 4-7: A zoomed-in view of the corresponding block diagram of the open-loop Gangway system as described in (4-13) to (4-14).

4-4 Nonlinear Model Predictive Control (MPC)

With the increase of computational power capabilities, MPC became a very active area of research, especially, because of its ability of to deal with Multiple-Input Multiple-Output (MIMO) systems while handling terminal constraints and systems limitations.
MPC problems are solved numerically since the analytical solution is mostly nontrivial. Hence, MPC requires a discrete-time mathematical model of the plant.
The derived model for the Gangway systems described in (4-14) is a nonlinear continuous-time model. The forward Euler method, for solving first-order differential equations, is considered here as the discretisation method, since it is intuitive and computationally efficient. Euler

method is given as

$$\dot{x} = \frac{x(k+1) - x(k)}{Ts}, \tag{4-16}$$

and the discrete-time state space equations becomes

$$x(k+1) = x(k) + T_s \ f(x(k), u(k), d(k)), \tag{4-17}$$

where k is the sampling time instance and T_s is the discretisation time step.
In the case of employing a linear dynamic model in an MPC framework, the MPC optimisation problem can be regarded as a convex problem and global optimum might be acquired. However, when the plant model is nonlinear, the optimisation problem becomes a nonlinear non-convex problem. Hence, solving the problem for the global optimum becomes computationally expensive and the global optimum is not guaranteed.
In case of the absence of constraints in an MPC problem, standard linear MPC. in essence, is merely a finite-horizon formulation of the Linear Quadratic Regulator (LQR) [53], in a sense that the control objective is to minimise a quadratic cost function along with a given time window. The length of the time window, in MPC, is referred to as the prediction horizon over which MPC predicts the system response upon a set of control input sequence.
Likewise, the nonlinear MPC follows the same logic of linear MPC, however, with nonlinear system equations and the formulation of the employed nonlinear MPC can be read as

$$\begin{aligned}
&\min_{\Delta U} \quad J(y(k), \Delta u(k)), \\
&\text{where} \\
&J(y(k), \Delta u(k)) \ = \ \sum_{i=1}^{N_p} ||Q \ (y(k+i|k) - r(k))||_2^2 + \sum_{i=0}^{N_c-1} \ ||R \ \Delta u(k+i|k)||_2^2, \\
&\text{subject to} \quad \begin{cases} x(k+1) \ = x(k) + T_s \ f(x(k), u(k), d(k)) \\ y(k) = h(x(k)) \\ u(k) = u(k-1) + \Delta u(k) \\ u_{min} \leq u(k) \leq u_{max} \\ \Delta u_{min} \leq \Delta u(k) \leq \Delta u_{max} \\ y_{min} \leq y(k) \leq y_{max} \end{cases} .
\end{aligned} \tag{4-18}$$

The objective here is to find manipulated variables ΔU that minimises the quadratic cost function $J(k)$ the most over the prediction horizon N_p at each time step. The cost function $J(k)$ is subject to a set of constraints including the Gangway system equations, boundaries on the input $u(k)$, the input increment $\Delta u(k)$, state vector $x(k)$, and on the system output $y(k)$. The optimisation manipulated variables ΔU are the input increment sequence $\{\Delta u(k|k), \cdots, \Delta u(k+N_c-1|k)\}$ over the control horizon N_c.
The optimisation runs at each time step k and tries to find the 'best' solution ΔU that minimises $J(k)$ the most and it is feasible with respect to constraints. This is achieved recursively where each generated solution is tested out by MPC. MPC predicts, using the plant model, the system response $\{y(k+1|k), \cdots, u(k+N_p|k)\}$ against the generated admissible set of the control input sequence $\{u(k+1), \cdots, u(k+N_c)\}$ over the prediction horizon N_p. Then, the corresponding cost function's value for the generated solution is computed.
The weighting matrices Q, R, described in (4-17), are the error tracking weights matrix and

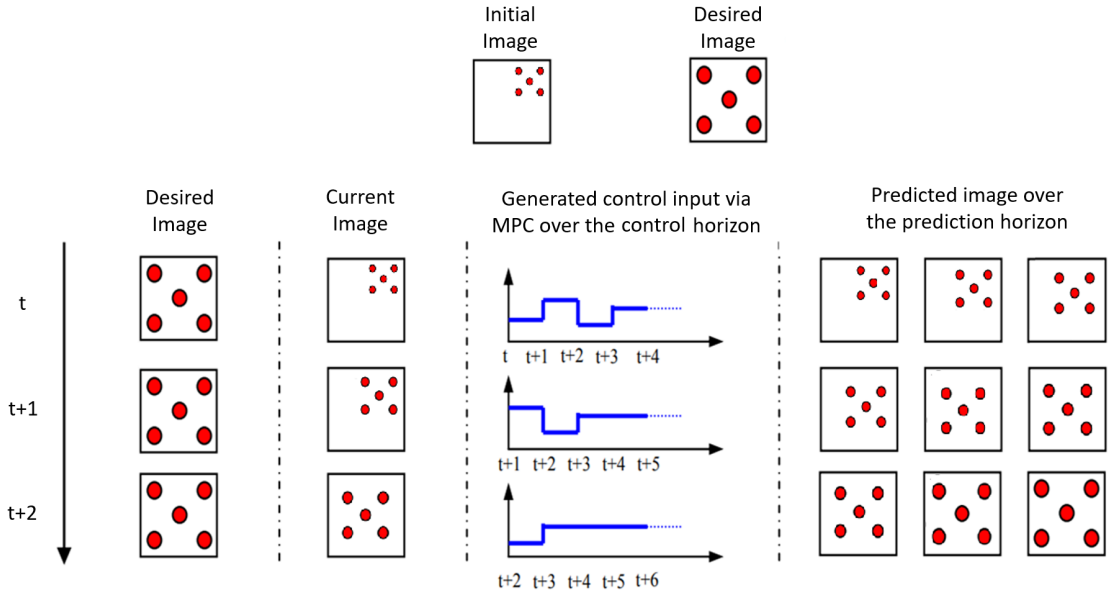

Figure 4-8: To the right, the predicted marker images over the prediction horizon (e.g. $N_p = 3$ for visualisation purposes). To the left, the plant actual response over multiple time steps $\{t, t+1, t+2\}$ to the left. (Reproduced) From [11].

the input effort weights matrix, respectively. The setpoint signal $r(k)$ is constant vector along the prediction horizon where it represents the desired location of the marker's corner within the desired field of view and the setpoint for the contact force, respectively.
Figure 4-8, depicts the predicted response over the prediction horizon against the actual plant response over multiple time steps. The system response is represented with which is represented by the observed marker features(i.e. the red dots) in the image plane. The marker appears initially in an arbitrary field of view. Then, evolves with MPC control commands to the desired field of view that corresponds to error-free of the Gangway tip 3D pose with respect to the target. Correspondingly, Figure 4-9 depicts the closed-loop of the MPC proposed method.

4-5 MPC parameters tuning

The main difficulty in MPC design lies in the number of parameters and settings that should be tuned to fulfil the control task requirements. Some of these parameters are often found by trial-and-error approaches some follows a general rule of thumb and others are merely based on the MPC designer's intuition.

4-5-1 Reducing the output variables

As it is described in the derived nonlinear model in (4-13), the output variables are the readily observed marker's features and the contact force measurements. The marker is the Aruco marker, given in Figure 3-7, which has its detected features represented by its centre

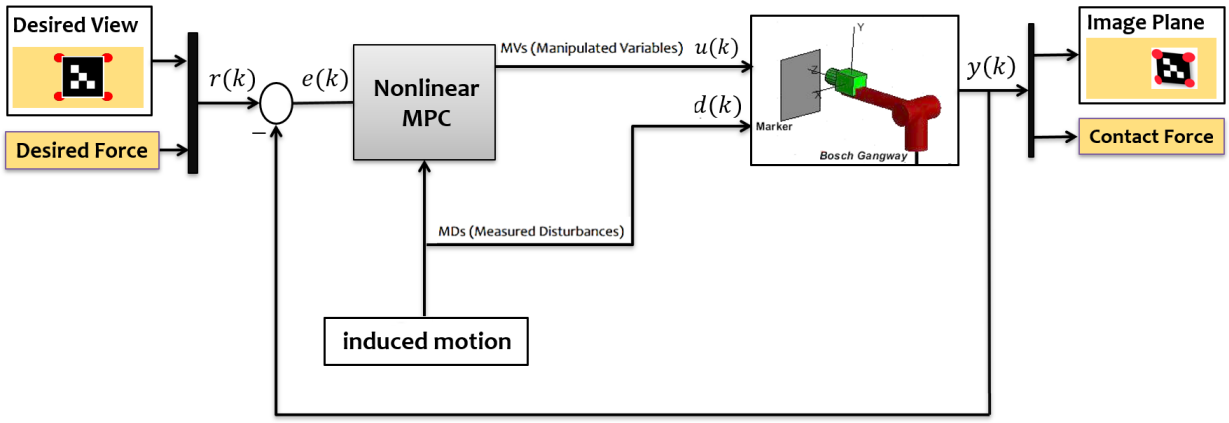

Figure 4-9: The nonlinear MPC scheme of for the task of automated docking.

and its four corners. During the design phase of MPC, it was noticed that choosing a set of three non-collinear points of the target would be beneficial in reducing MPC computational burden while demonstrating the same level of performance in case all target features are considered. Thus, the MPC-model output is reduced where only, besides the contact force measurements, the centre of the marker and its lower corners were considered.

4-5-2 Sampling time

Choosing a large time step T_s might not be enough to capture the system dynamics and having a very small time step will increase computational power demands in the MPC scheme. To select a proper time step value h. A general rule of thumb is to have 4 to 10 samples per rise time of the step response of the discretised system [54].
The approximation of the low-level closed-loop dynamics of the gangway system G_{ss}, as described in (4-8) and (4-10), is the slow part of the derived model dynamics in (4-14). Additionally, having a vision sensor in the control loop imposes an extra limitation of choosing a small value for T_s. Camera latency for detecting and tracking the target (i.e. the marker) can be as low as (20 to 30 ms). Therefore, the time step was chosen as $T_s = 0.02$ sec according to Table 4-1.

Table 4-1: Selecting a proper time step

Sampling time T_s (sec)	Number of samples per rise time (-)
0.02	6
0.025	4
0.03	3

4-5-3 Prediction and control horizons

The prediction horizon N_p is basically the length of the time window over which MPC predicts the plant model response. The higher the value for N_p the more computational power needed to solve the MPC optimisation problem. Also, a high N_p value leads to less aggressive system response. Because when prediction horizon N_p is large, MPC has more observations on the system response hence the optimisation problem might find a better solution. However, increasing N_p to certain value no improvement in the overall performance was observed. Correspondingly, low N_p value can reduce the required computational effort however, it leads the system to behave more aggressively.
Furthermore, high value for the control horizon N_c determines the length of the manipulated variables vector ΔU along the prediction horizon, which implies $N_c \leq N_p$.
Increasing the control horizon N_c can result in less aggressive control input and more relaxed with respect to the saturation limit. Also, N_c plays a crucial role in increasing the optimisation problem complexity, thus, increasing the required computational effort drastically. On the other hand, setting a low value to N_c can reduce the computational effort but might lead to a more aggressive response.
Based on that, via a trial-and-error approach, N_p and N_c values were tuned accordingly. More details about the numerical experiments of this tuning process can be found in Chapter 5.

4-5-4 Input and output weights

The weighting matrix Q, described in (4-17), is a diagonal matrix where each item corresponds to how much emphasis MPC should put on one particular output of the system. For instance, to enable automated docking in a hierarchical fashion, the control task was categorised into two main parts; tracking the target (i.e. the offshore platform) and docking into the target. Hence, more emphasis is put on the centre of the marker because, according to the design objectives, minimising the error in the image plane of between the desired field of view and the detected marker's features results in minimising the relative spatial velocity between the gangway tip and the target.
Correspondingly, when the docking is enabled the contact between the Gangway tip and the structure is initiated. Since the exerted force by the Gangway should not exceed certain limits to avoid damaging the structure and maintaining the contract with the offshore platform. The contact force associated weight is the most important one, see the last item in Q in (4-19)
Furthermore, the weighting matrix R is also a diagonal matrix that penalties the input increment vector $\Delta u(k)$. Let us recall, that $u(k)$ is the control input vector to the system which represents the Gangway tip velocity in 3D space. High associated value to a particular input will result in a 'sluggish' response on the output channels that are associated with that particular input.
However, setting the associated weight of this particular input to a low value will result in a more sensitivity on the associated output channel which might potentially affect the robustness. For instance, while the tip is in contact with the platform it is important to keep tracking the contact force while tracking the target motion (i.e. compensating the sea-induced motion). This means if the target moves along the sway axis the telescoping joints should track this motion while assuring that the exerted force at the tip still with permissible limits.
Moreover, the ratio between the output and input weights Q/R determines the aggressiveness

and robustness of the controller performance (e.g. in disturbance rejection) [53].
Accordingly, Q and R values were found via a trial-and-error process based on judging the corresponding performance of the contact force response (in terms of fluctuation).

$$Q = \begin{bmatrix} 2 & 0 & 0 & 0 & 0 & 0 & 0 \\ 0 & 0.5 & 0 & 0 & 0 & 0 & 0 \\ 0 & 0 & 2 & 0 & 0 & 0 & 0 \\ 0 & 0 & 0 & 0.5 & 0 & 0 & 0 \\ 0 & 0 & 0 & 0 & 5 & 0 & 0 \\ 0 & 0 & 0 & 0 & 0 & 5 & 0 \\ 0 & 0 & 0 & 0 & 0 & 0 & 20 \end{bmatrix}, R = \begin{bmatrix} 0.5 & 0 & 0 \\ 0 & 0.2 & 0 \\ 0 & 0 & 0.5 \end{bmatrix}. \tag{4-19}$$

Recall that, the output vector $y(k)$ in the derived model in (4-15) is the corners, the centre of the marker, and the contact force response, respectively. Where each marker feature has two coordinates (i.e. location in the image plane). In Section 4-5-1, however, the output vector is reduced to 7 channels where only the lower concerns, the centre of the maker, and the force response were considered in the MPC-embedded model. Thus we see, in the last three items in the principal diagonal of Q, that the weight values were selected to be highest since they are associated the centre of the marker and the force, respectively.
Note that, the second weight in the R matrix is associated with second input to the system, namely the Gangway tip velocity along y-axis. Which is translated into a velocity command for the telescoping joint through the inverse Jacobian matrix, as described in (4-14).

4-6 Perturbations anticipation

As described in the derived model (4-13) and depicted accordingly in Figure 4-7, the sea-induced motion that acts on the vessel is mapped out to the target reference frame and it is incorporated within the nonlinear model where it can be regarded as external perturbations that act on the system.
In Figure 4-9, the MPC block takes in these perturbations, denoted by 'induced motion' block, as a measured disturbance signal. The formulation of the MPC problem, described in (4-17) lets the MPC scheme enjoys the anticipatory property in case the measured disturbance signal is available for more than one-time instance k along the prediction horizon N_p.
Although, in the simulation environment, it might be 'natural' to feed the MPC block with multi-step-ahead of the measured target motion (sea-induced motion) with the available data set. This is not the case however in reality, where MRU is providing a single reading at each time step.
In Chapter 2, it is stated that predicting the incoming waves is possible using wave spectra and historical readings. However, when the vessel reaches the offshore platform the vessel's bridge turns on the Dynamic Positioning (DP) system which tries to maintain a fixed distance to the offshore platform while counteracting the sea-induced motion. This motion compensation system is not perfect and results in residual motion mainly along the horizontal plane. Thus, the incoming induced motion is distorted because of the DP system and the radial forces between the vessel and the offshore platform. Thus, forecasting the incoming waves using wave-spectra techniques is pointless.

Accordingly, in this thesis, a data driven approach for forecasting the induced motion is designed. This multi-step-ahead forecasting scheme is based using historical data of the MRU measurements.
This is achieved, first, by training a neural network with NARX topology (Nonlinear Autoregressive model with Exogenous inputs). Then, the trained NARX function is employed in the control loop. Where it provides the MPC block with a prediction sequence of the disturbance variable $d(k)$ along the prediction horizon N_p.
NARX is a multi-layer of feedforward neural network with an architecture of Recurrent Neural Network (RNN). NARX is a popular technique for estimating the dynamics of a nonlinear system (i.e. black-box identification) [55]. Where it employs tapped delays of the input variable to resemble a memory of the system dynamics. For a multi-step-ahead prediction of a time series, it is recommended to feed the previous output of the neural network as an input channel [55]. NARX can deliver a good performance for multi-step-ahead prediction in case of univariate forecasting problem. Where for multivariate problem poor performance is reported [56].
The sea-induced motion affects the system mainly along the translational axes. Hence, three variables need to be forecasted. To gain higher performance, three NARX neural networks were trained separately to perform the prediction for each axis of motion. MPC utilises these prediction to substitute $d(k)$ values along its prediction horizon N_p. Therefore, the prediction horizon for the induced motion N_d should not exceed N_p. The design of each neural network along each axis of motion is identical. Where the input for the neural network is the MRU velocity readings at time instance k. With each neural network is designed preforms three-step-ahead prediction. Hence, the supplied disturbance sequence to the MPC block is $\{d(k|k), \cdots, d(k+3|k)\}$, which corresponds to $N_d = 4$.
A data set of the MRU measurements were used to train these neural networks. The data set were divided into three batches; 70% for training, 15% for cross-validation, and 15% for testing. This is a common practice in training the neural network to avoid overfitting regularisation [55]. The training was performed with MATLAB Deep Learning Toolbox. The performance metric for training and validation is chosen as Root Mean Square Error (RMSE) which is a gradient defined function (smooth function), RMSE is given in terms of the prediction error as

$$RMSE = \sqrt{\frac{1}{n}\Sigma_{i=1}^{n}\Big(e\Big)^2} \tag{4-20}$$

Each neural network preforms three-step-ahead prediction with three output channels (an output channel for each prediction step). Figure 4-10 is a MATLAB-generated diagram of the designed NARX neural network topology. Where the hidden layer utilises 30 neurons with one input variable $x(t)$ (the forecated variable) and the output feedback vector $\{y(t+1), y(t+2), y(t+3)\}$ (three-step-ahead prediction).
High performance (i.e. low RMSE value) is recorded, when the tapped delays of the forcaseted input variable $x(t)$ are set to; $\{x(t), x(t-1), \cdots, x(t-10)\}$. For feedback coming from the prediction output vector $y(t)$ one tapped delay is chosen, which results in shifting the prediction vector one step back $\{y(t), y(t+1), y(t+2)\}$. Where t refers to the time instance of the MRU measurements.
Once the neural network showed a proper performance, the designed neural networks were validated on another data set to avoid confirmation biased. Figure 4-11 shows the neural network forecasting error of the sea-induced motion (velocity) along the surge, sway, and

heave axes. With the corresponding RMSE value along each axis, respectively.

$$RMSE = \begin{bmatrix} 0.0030318 & 0.010249 & 0.0066153 \end{bmatrix}$$

After applying this scheme, a noticeable enhancement in the performance in the contact force task was observed. Chapter 5 discusses more in-depth the effect of the anticipatory action on the performance.

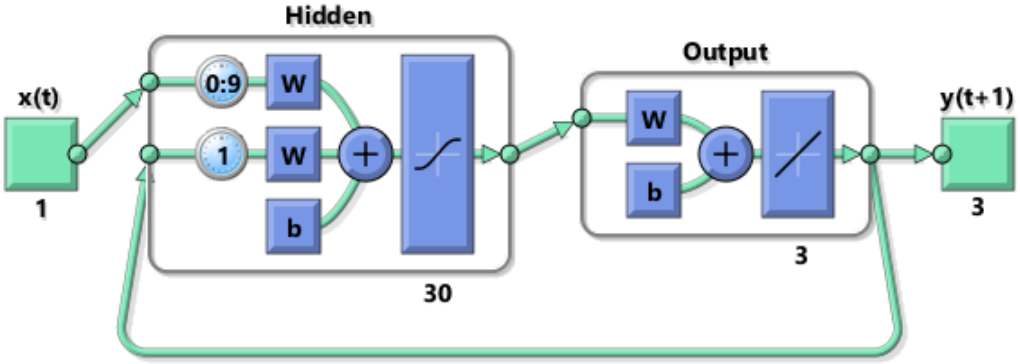

Figure 4-10: The designed architecture of the employed NARX neural network.

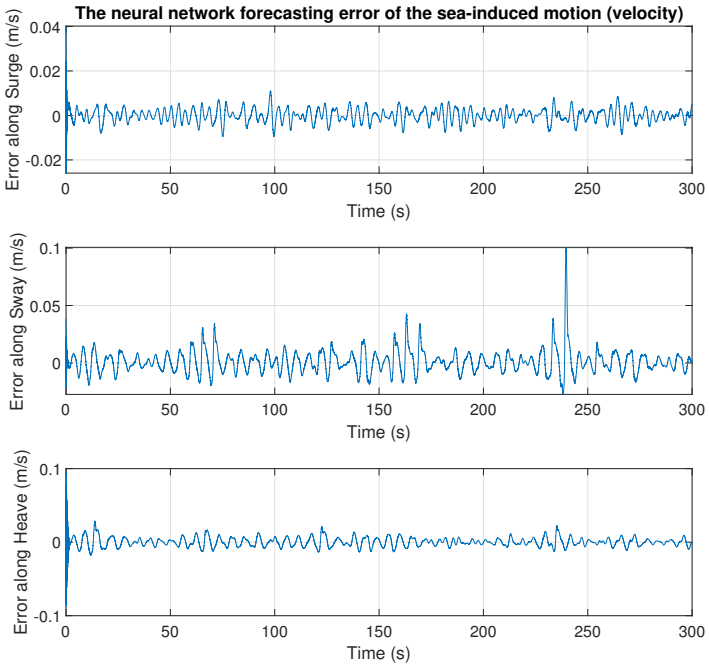

Figure 4-11: The neural network forecasting error of the sea-induced motion (velocity).

4-7 Closed-loop stability analysis

The cost function $J(k)$ in the MPC block, described in (4-17) is a quadratic cost function which has, by implication, a positive value. In [53, 57], M. Lazar *et al*, provide intuitive proof for the endpoint convergence in the quadratic MPC closed-loop scheme. By assuming, a Lyapunov cost function that is equivalent to the MPC's cost function $J(k)$.
We recall, if a function is positive definite and it is a monotonically decreasing function, then, the cost function is considered to be a Lyapunov function candidate [58].
In Figure 4-12, one can see that the value of cost function, decreases asymptotically over the experiment time. This may indicate that the cost function is a Lyapunov function candidate since it is also positive definite by its nature. Consequently, this would have proved global stability of the closed-loop system in case of the cost function is not a subject to constraints. Thus, one cannot conclude the global stability but rather the endpoint convergence of the closed-loop system.

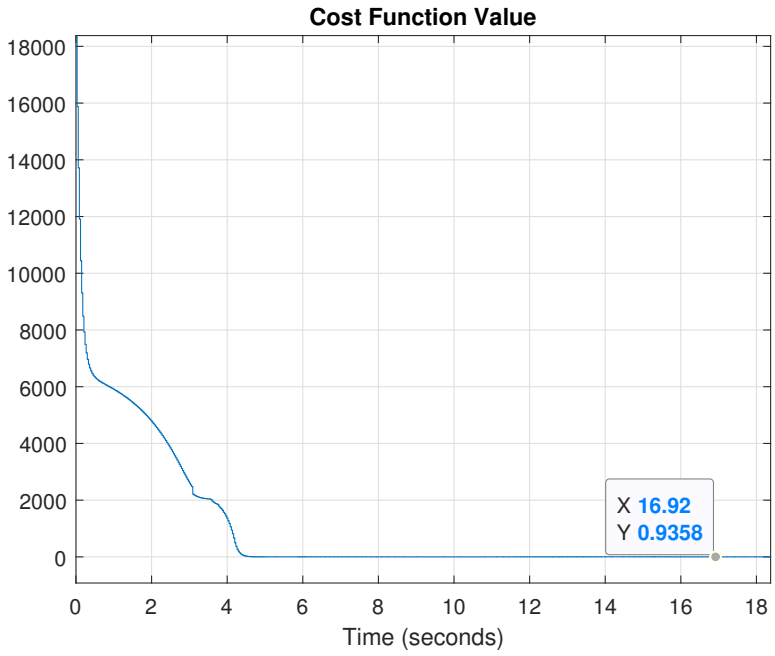

Figure 4-12: The cost function value.

4-8 Summary and discussion

In conclusion, this chapter answers the research questions regarding incorporating the vision sensor in a high-level control scheme to enable the automated docking scheme.
After reviewing the current development and the classical approaches in the literature, a 'high-level' control scheme was proposed. This control scheme is mainly based on the standard nonlinear MPC as a control strategy.
The novelty in this work lies in deriving a mathematical model of the Gangway system that

is suitable for the MPC scheme with fulfilling the control task requirements. Moreover, a neural network with NARX architecture was designed and trained to perform multi-step-ahead forecasting of the MRU readings. This can enable the anticipatory property within the MPC scheme which enhances the contact force response.
Overall, it may be said that this method offers a singularity-free solution for a vision-based control task (i.e. the automated docking problem) while handling system constraints (e.g. the workspace) and the control objective constraints (i.e. contact force response). However, the proposed control method is computationally expensive and further research is required, hence, for now, this is regarded as a major drawback, especially, from the industry perspective.

Chapter 5

Results

This chapter evaluates the performance of the proposed MPC solution for automating the docking procedure of Bosch's Gangway system. The controller is first tested for the nominal case with multiple scenarios (i.e. with and without disturbance anticipation, different prediction and control horizons N_p and N_c values). Then, tests are performed against plant model mismatch. Lastly, the performance is evaluated for a more extreme case in terms of the amplitude of the sea-induced motion.

5-1 Nominal Case Scenarios

This section discusses the performance of the employed nonlinear MPC scheme in Chapter 4. These scenarios are evaluated with the nominal plant model (i.e. no model mismatch).

5-1-1 No disturbances case

First, the nominal case scenario evaluates the proposed control scheme performance in case no disturbances are applied to the system. This means the amplitude of the sea-induced motion is set to zero. In the real world scenario, this case does not exist. Nevertheless, this trial is beneficial since it provides the baseline evaluation of the proposed controller in the simulation environment.
This test was attained in two trials with different initial conditions (i.e. various relative poses between the Gangway tip and the target). In this project, it is supposed that the initial conditions of the Gangway are fixed to certain values. In practice, this holds since the vessel's bridge has a communication channel with the Gangway system. Hence, coordination between the vessel's Dynamic Positioning (DP) system and the Gangway's joint-level control system is possible. In the current system, this coordination happens between the vessel's bridge and the Gangway's operator [7]. Accordingly, in order to enable the automated docking, this project proposes direct coordination between the Gangway joint-level control loop and the vessel's bridge such that the target is within the camera field of view once the automated docking is

initiated.
Therefore, the initial value of the joint displacement vector q_g for all the tests in this Chapter is fixed to the value $q_g = [q_{slew}, q_{luff}, q_{tele}] = [90°, 90°, 17m]$. The case of no disturbances (i.e.

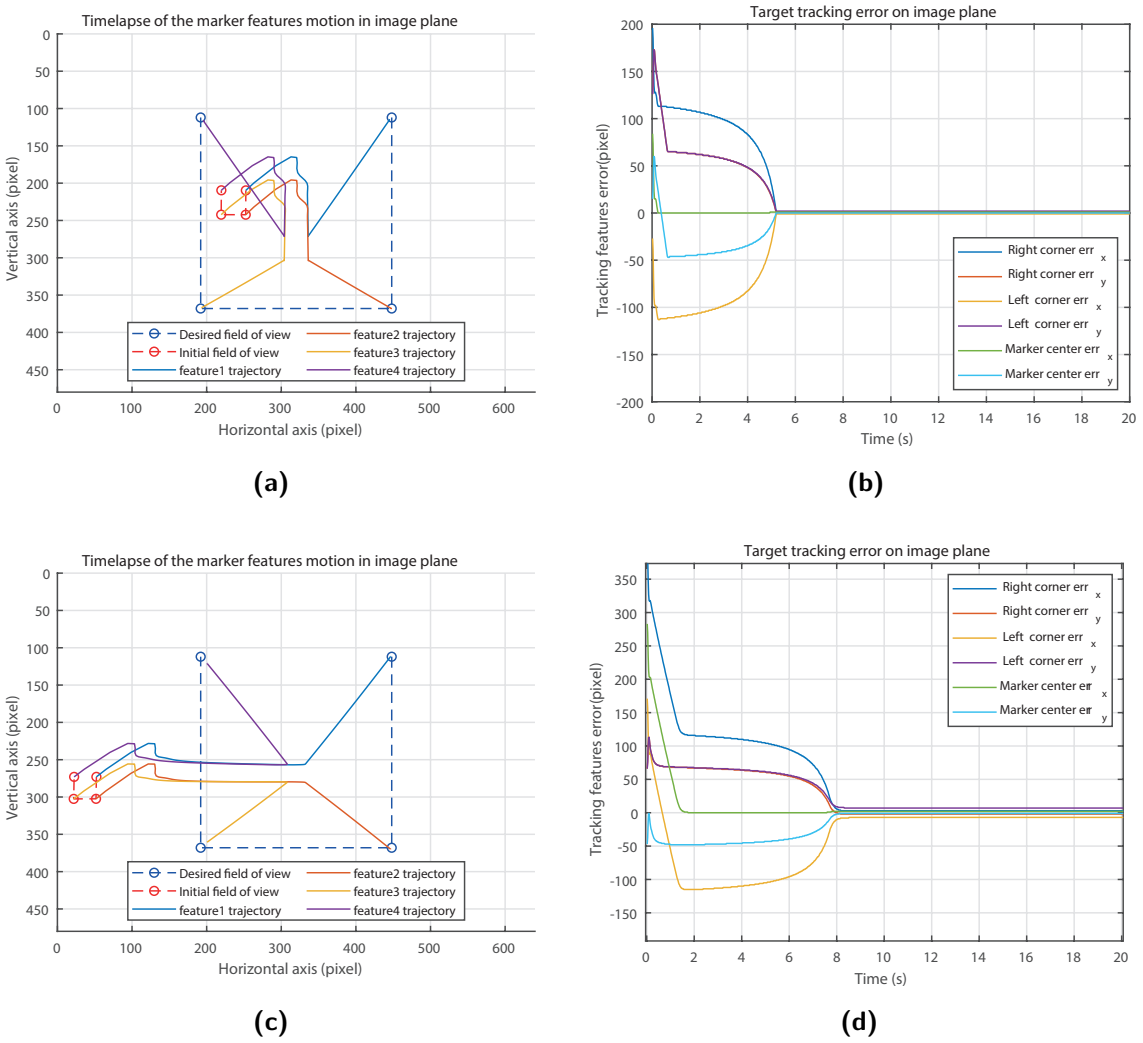

Figure 5-1: Here, the target is stationary with a relative position, to the Gangway base, of $P_{target} = [0.5, 23, 1]^T$ in case of (a) and (b), and $P_{target} = [4, 25, 2]^T$ in case of (c) and (d). (a) and (c) illustrate time-lapse footage of the target (marker) detected features in the field of view over 20 seconds. (b) and (d) show the corresponding tracking error of the target features in the 2D image plane.

no induced motion) means that the target is stationary with respect to the Gangway base. The first set of initial conditions, denoted by x_{00} in Figure 5-2, is the target pose P_{target}, as described in (4-14), in 3D space with respect to the Gangway base reference frame is set to $P_{target} = [0.5, 23, 1]^T$. Figure 5-1a, shows time-lapse footage of the target (marker) detected features in the field of view. We recall that in the proposed control scheme the camera is placed on the Gangway tip, see Figure 3-10. Consequently, we can see, in Figure 5-1a that in the initial field of view, the target (red dashed-square) appears in a 'small' size. This size corresponds to the distance between the target and the camera optical axis, see Figure 3-3 in

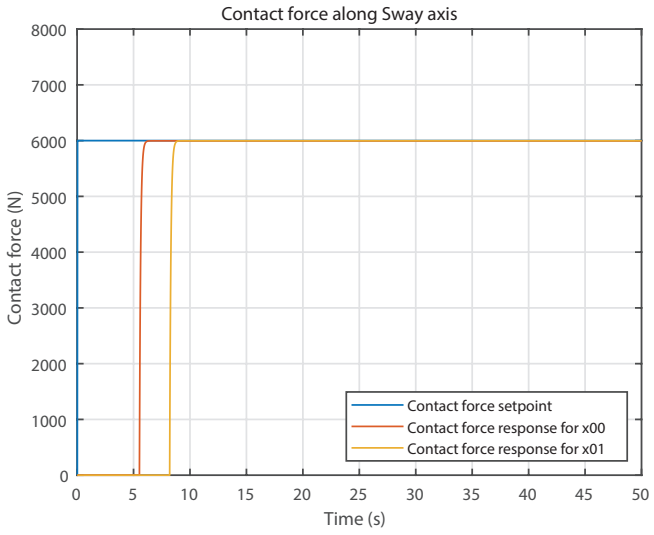

Figure 5-2: The corresponding contact force response of the first and the second initial conditions set denoted by x_{00} and x_{01}, respectively.

Section 3-3.
In the MPC scheme, higher weight is put on the centre of the marker than the corners associated weights, as described in Section 4-5. The MPC scheme considers a higher priority to the task of tracking the marker centre. Hence, MPC aims to align the marker in the centre of the desired field of view, by manipulating the rotational joints of the Gangway. Once the marker centre reaches the desired location in the image plane, MPC manipulates the telescoping joint which has the zoom-in effect on the field of view since the camera is attached to the tip. Moreover, the desired field of view represents the constant setpoint signal $r(k)$ and it is chosen such that the 3D displacement error between the tip and the target is zero (i.e. the case of docking).
The corresponding tracking error of the target features in the image plane is shown in Figure 5-1b.
The second set of initial conditions, denoted by x_{01} in Figure 5-2, the target pose P_{target} in 3D space with respect to the Gangway base reference frame is set to $P_{target} = [2, 25, 2]^T$. In this case, the initial target location is even more distant than in the first case. Hence, the marker appears even smaller in the initial field of view, see Figure 5-1c. The corresponding tracking error of the target features in the image plane is shown in Figure 5-1d.
Correspondingly, the contact force response for both the first and the second set of the initial conditions is depicted in Figure 5-2. Notice that, in the second set, the target is more distant to the Gangway tip. Therefore, the automated docking task takes more time than in the first case. as shown in Table 2-2, to guarantee a connection between the Gangway tip and the offshore platform, and to avoid damaging the structure, the contact force response should be between (4000-8000 N). Therefore, the force setpoint is chosen in the middle of the allowed range as (6000 N) to safeguard against response fluctuations.

5-1-2 Adding disturbances

After demonstrating the baseline performance of the proposed control, we need to test the performance in the case of induced motion which better represents the real-world scenario.
As Section 4-3-4 states, it is expected that providing the MPC with the induced motion measurements as a measured disturbance channel is essential to achieve the control task of contact force regulation. This is demonstrated and confirmed indeed in this trial, see Figure 5-3.
Figure 5-3a illustrates time-lapse footage of the target (marker) detected features in the field of view over 25 seconds. Where the target 3D displacement is shown in Figure 5-3d. The target motion is caused by the sea-induced motion. However, this induced motion was not provided to MPC. Therefore, the target poorly tracked to the desired field of view and control force requirements is not fulfilled, as shown in Figure 5-1c. Notice that, in Figure 5-3b, during the first five seconds the performance of the tracking control is similar to the case of a stationary target. This is mainly due to the perspective projection effect along the optical axis. Where the motion of a distant object from the camera results in a much smaller deviation in the image plane.
Thus, based on the results of the previous test, the induced motion measurements are provided to MPC as a measured disturbances channel $d(k)$, as described in (4-17) Where every time instant k, the MRU readings is provided to MPC. However, MPC predicts the system response over the prediction horizon window. Thus, the provided value for $d(k)$ is held constant in the predicted model along the prediction horizon and only updated in the next time step with a new MRU reading.
Figure 5-4a shows the contact force response when the sea-induced motion is present in the system and provided accordingly to MPC via MRU readings at each time instance. The force response is fluctuating, however, within the allowed range. Correspondingly, in Figure 5-4b the tracking error in the image plane is shown. Hence, by comparing the system responses in Figure 5-3 and 5-4, we can say that providing the MPC with the MRU readings is crucial to obtain the control task requirements while tracking the target motion.

5-1-3 Disturbance anticipation

As stated in Chapter 4, enabling the disturbance anticipatory action in the MPC scheme should enhance the overall preference. Accordingly, a neural network with NARX topology was designed and trained for the purpose of anticipating ahead the induced motion.
Indeed as expected, by supplying MPC with the induced motion predictions, MPC force response is improved. Figure 5-5 shows the contact force response in case of no disturbance anticipation, disturbance anticipation with the induced motion data set provided by Bosch, and the force response with the trained neural network. Clearly, in case of anticipating ahead the induced motion, the fluctuation in the force response is attenuated compared to the case of no anticipation. Moreover, the force response using the neural network is similar to the force response using the data set. However, these two responses are not identical due to the prediction error in the neural network as seen in Figure 4-11.

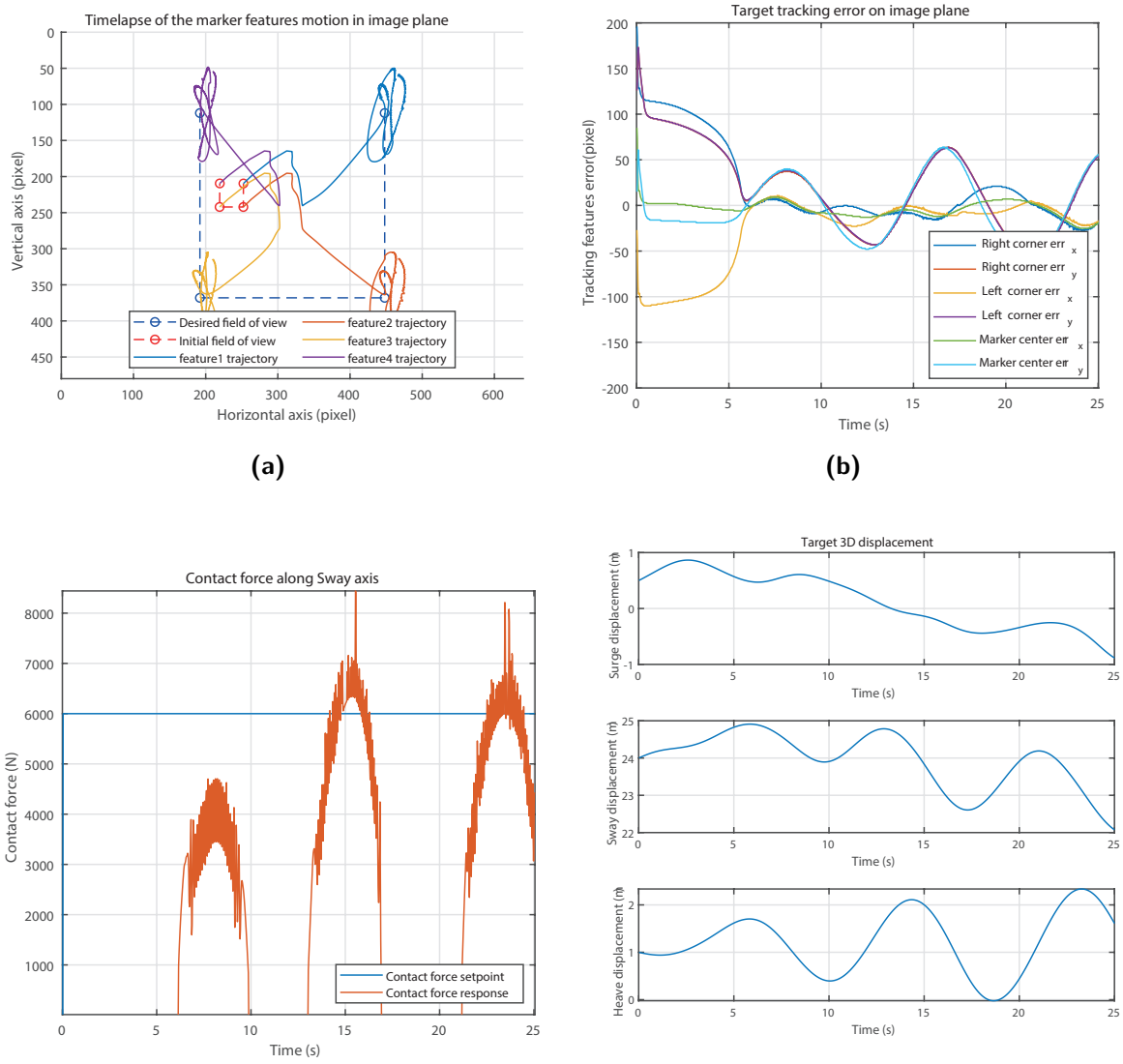

Figure 5-3: This set of figures corresponds to the case where the induced motion is present on the system, however, MPC has no access to these data. Correspondingly, MPC shows poor performance in tracking the setpoints. Therefore, the target visual information coming for the camera is not enough and MRU readings are needed. (a) and (b) illustrate time-lapse footage of the target (marker) detected features in the field of view over 25 seconds and the corresponding tracking error, respectively. The corresponding contact force response and the target pose is depicted in (c) and (d), respectively.

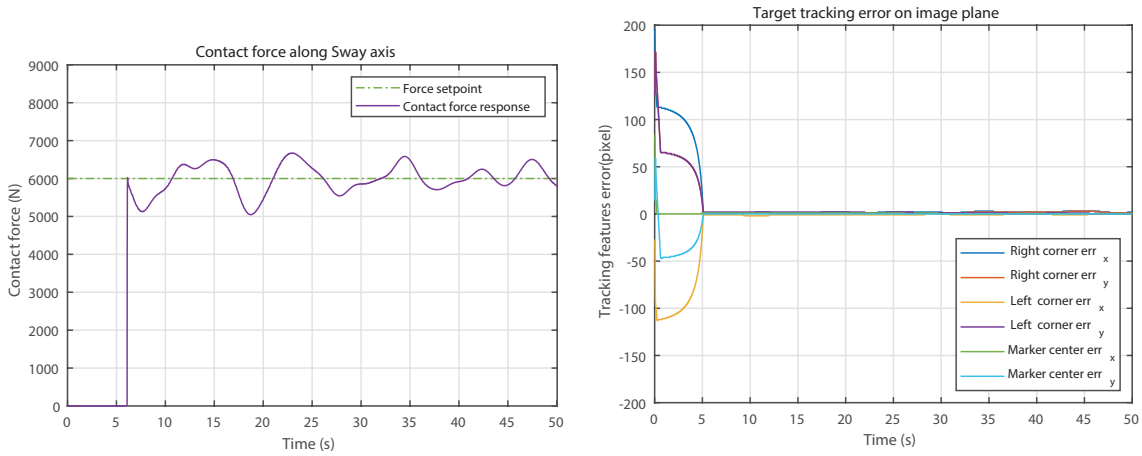

(a) **(b)**

Figure 5-4: This figures corresponds to the case where the induced motion is present on the system and provided accordingly to MPC at each time step (instant feedback). The contact force response for this case is shown in (a). The corresponding target's features tracking error is shown in (b).

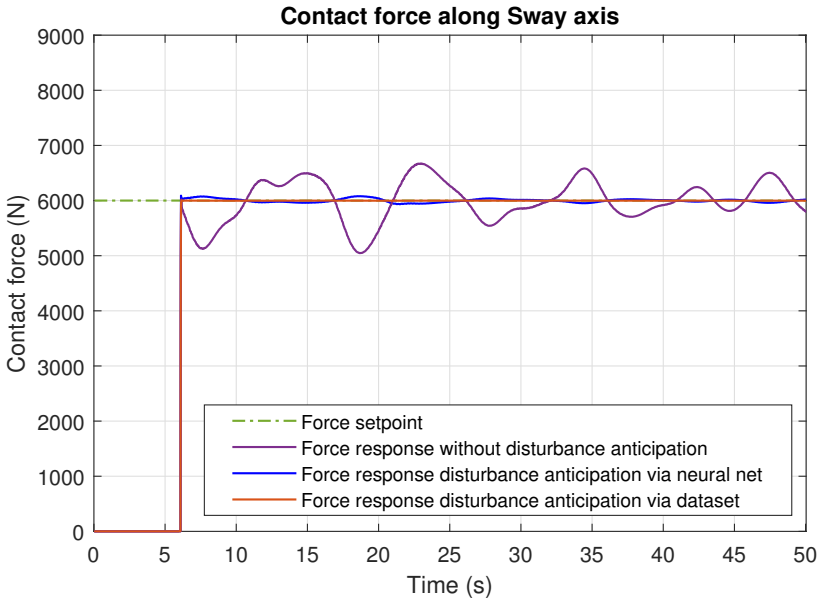

Figure 5-5: The contact force response in case of; no disturbance anticipation (nominal case), disturbance anticipation with the induced motion data set, and disturbance anticipation with the trained neural network.

5-2 Selecting prediction & control horizons values

One of the challenging points in implementing an MPC scheme is the degrees of freedom MPC has in terms of the tuning knobs (e.g. prediction and control horizons, input and output weights).
In this project, the selection of the MPC parameters is based on an iterative process of trial-and-error and general guidelines for MPC tuning in [54, 59].
Thus, several trials were performed to evaluate the proposed MPC scheme against different prediction and control horizons N_p and N_c, respectively. The results of these trials indicate the impact of increasing/decreasing N_p, N_c values on the overall performance.
Choosing values for these parameters affects not only the controller performance but also the computational complexity of the MPC algorithm which solves an online optimisation problem at each time step.
In the work of Garriga and Soroush [54], a literature review is presented over the techniques and the general guidelines for tuning MPC parameters. A general rule of thumb is to set the prediction horizon as ($T_{set} \leq N_p T_s$). Where T_s is the chosen sampling time, and T_{set} is the settling time of the open-loop step response. Recall that, the low-level plant dynamics $G(s)$, described in (4-8), is the slow dominant part of the Gangway system dynamics. The settling time of a second order system can be given as, [60],

$$T_{set} = \frac{4}{\zeta \omega_n} = 0.065$$

Thus, in this set of trials the initial value for

$$\frac{T_{set}}{T_s} = 5 \leq N_p$$

The control horizon is the set of future admissible control actions leading to this predicted plant output. Usually, the control horizon is set as $N_c < N_p$. Where the rest of the inputs are held constant along the prediction horizon.
For this set of trials, MPC shows nearly identical performance in tracking the target in the image plane while differing in the calculation time. However, the impact of choosing different values for N_p, N_c can be significantly observed in the contact force response.
Figure 5-6, depicts the contact force response for different values of N_p, N_c. The corresponding target pose for this set of trials is depicted in Figure 5-7. Figure 5-6a, evaluates the contact force response for different N_p values and a constant N_c value. Note, the scale of the vertical axis is enlarged compared to the one depicted in Figure 5-6b. When choosing a proper value N_c (i.e. $N_c = 3$) the performance gain of the different N_p values is insignificant. Whereas, N_c value has higher impact on the force response, see Figure 5-6b. Setting a small value for N_c (i.e. $N_c = 1$) leads MPC to perform worse against incoming disturbances. Thus, we see a fluctuation in the force response when $N_c = 1, 2$. However, the impact on the force response of choosing any value of $N_c > 3$ is insignificant and only increases the optimisation problem complexity. In this set of trials, the disturbance anticipatory property in the MPC was enabled using the provided data set.

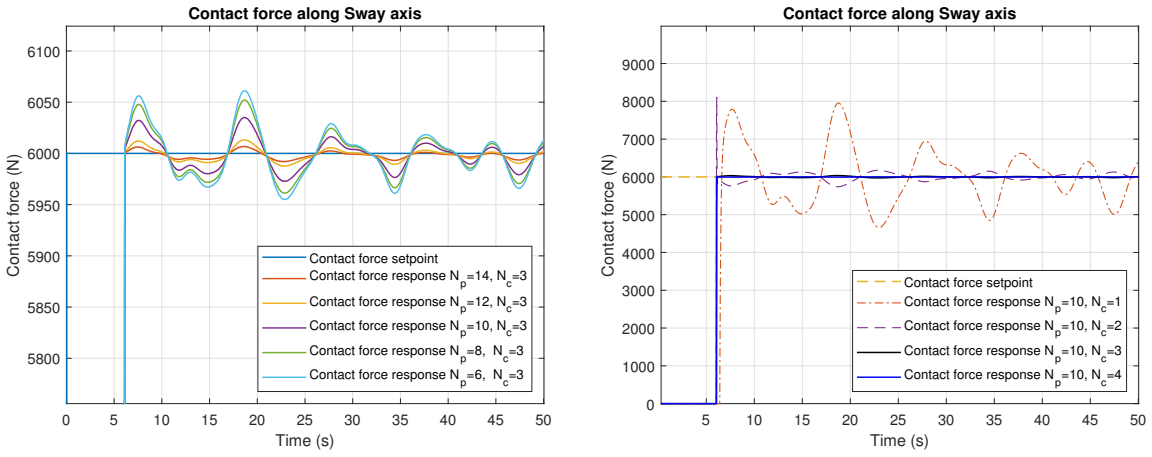

(a) **(b)**

Figure 5-6: The contact force response for different N_p values (a), and different N_c values (b). Note, the scale of the vertical axis is enlarged in (a) compared to the one depicted in (b).

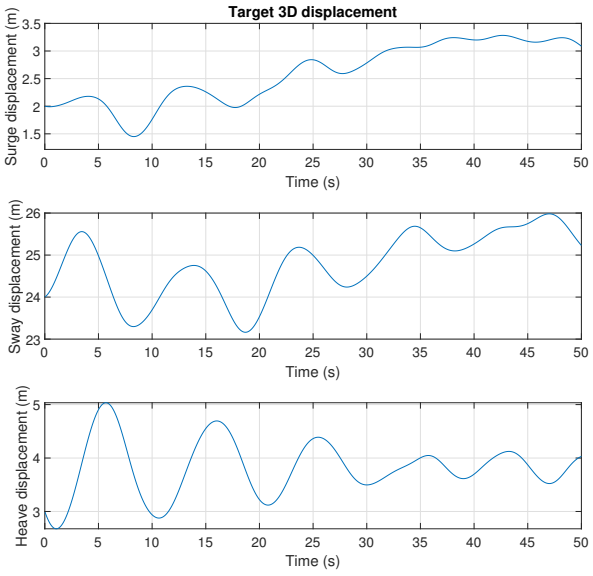

Figure 5-7: The corresponding target pose.

5-3 Model mismatch tests

The previous test scenarios were performed to evaluate the proposed control method in terms of fulfilling the control task objectives. Likewise, in this section, the robustness of the proposed MPC scheme is evaluated through a set of trials that involves a model mismatch between the MPC embedded model and the plant model. In this set of trials, the disturbance anticipatory property in the MPC was enabled using the provided data set. The prediction horizon was set to $N_p = 8$, and different control horizon values were test $N_c = 2, 3$.

5-3-1 Output parameters mismatch

The measurement system of the proposed control scheme employs a monocular camera and a force sensor at the tip. The output of these sensors might vary compared to the MPC embedded model. This variation is caused by operating conditions such as vibrations, fatigue, and sensor misalignment.

- **Bumper stiffness mismatch test**
  The rubber bumper at the tip has a linear stiffness coefficient estimated by Bosch around the operating window. However, fatigue and other operating conditions may cause a variation in the stiffness coefficient K_b, introduced in (4-10), of the rubber bumper which leads to a variation in the contact force response.
  Accordingly, a set of trials were run to evaluate the impact of the stiffness coefficient variation on the contact force response. As part of the iterative tuning processes, these trials were performed for different control horizon N_c values. Figure 5-8 depicts the corresponding contact force response when the stiffness coefficient K_b has a mismatch of $\pm\%5$ from the nominal model. This trial was performed for $N_c = 2, 3$, as part of the iterative tuning process of MPC, and beyond these values for N_c no gain in performance was observed.
  Clearly, the impact of the stiffness mismatch on the force responses is linear and proportional to the mismatch percentage. When $N_c = 3$ MPC yields better disturbance rejection. Where the fluctuation in the force response, caused by the target motion, is attenuated.

- **Camera misalignment test**
  As Chapter 3 concludes, the camera is attached nearly at the tip of the Gangway. Often, in vision-based robotic manipulation tasks, a precise calibration between the camera and the robot end-effector is needed to eliminate the error in the target pose estimation. However, in the proposed control scheme the target is detected and tracked within the 2D image plane. Thus, the relative pose estimation problem is solved implicitly by matching the target image with the desired field of view. This concept is enabled in the scheme of Image-Based Visual Seroving (IBVS), as stated in Section 4-1. As a consequence, IBVS schemes enjoy robustness properties against the camera calibration error [8,47]. The proposed control scheme also tracks the target in the 2D image plane. Hence, correspondingly, the proposed scheme is expected to be pron against camera calibration error. This is demonstrated and confirmed indeed in this trial, see Figure 5-9.
  In this trial, the camera position is misaligned by ± 10 cm on along the principal axes. Figure 5-9 shows a time-lapse over 50 seconds of the target in the image plane and the corresponding features tracking error in 5-9a and 5-9b, respectively. Notice, even a small misalignment (i.e. ± 10 cm) in placing the camera at the tip can lead to big shift for the final marker location in the field of view. This is caused by the perspective projection in the employed vision sensor.
  On the other hand, in this trial, the contact force response followed the force setpoint without any offset, see Figure 5-9c. This is mainly due to the way the output weights matrix Q was constructed in MPC. As stated in Section 4-5, a higher weight value is chosen to put more emphasis on the force output channel since it is more vital for

maintaining the contact with the target. Moreover, the corresponding error along the principal axes between the Gangway tip and the target is depicted in Figure 5-9d.

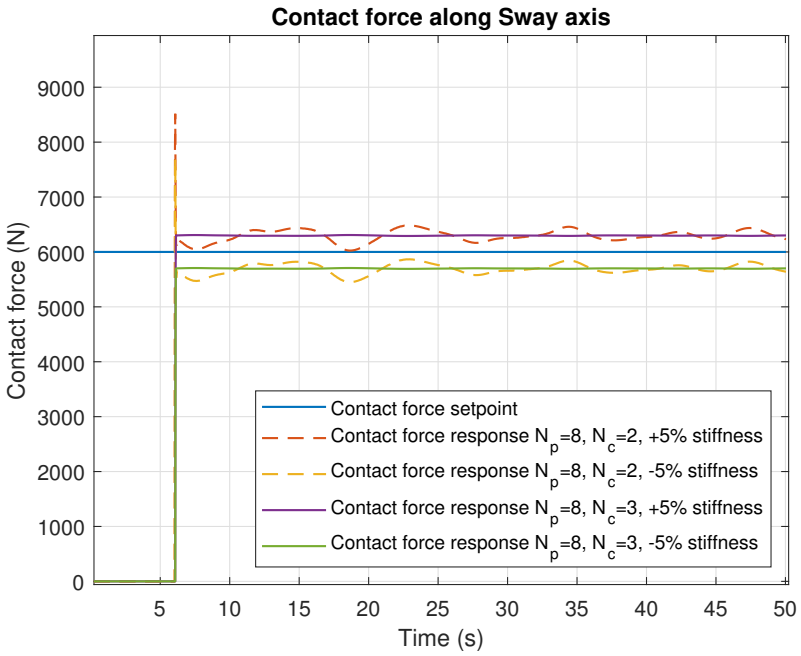

Figure 5-8: The corresponding contact force response for different N_c values in case of stiffness coefficient K_b mismatch.

5-3-2 Plant dynamics mismatch

In this thesis, the derived model parameters of the Gangway system was provided by Bosch according to their design (e.g. the Gangway geometrical dimensions). Bosch also provided an approximation of the closed-loop dynamics of each controlled joint in the Gangway system. However, this approximation is based on their intuition of their system performance (the numerical experiments may be carried in future work). Hence, testing the proposed scheme with this approximation mismatch is an interesting case scenario. The approximation of the low-level closed-loop equivalent system is a second-order transfer function with a bandwidth of $\omega_n = 6$ Hz, as described in (4-9). An interesting test scenario is to evaluate the performance of the proposed MPC in case of plant dynamics mismatch.
Figure 5-10 depicts the contact force response for different dynamics mismatch cases.
As stated in Section 4-3-4, MPC can incorporate in its scheme the different constraints the system is subject to. However, setting all the system constraints are set as hard constraints may lead the optimisation solver to an unfeasible solution. Accordingly, the system input associated constraints are set as hard constraints (i.e. to avoid introducing instability) and the output constraint are relaxed into soft constraints by introducing a slack variable $\epsilon \geq 0$. Where introducing soft constraints is a common practice in MPC design to avoid unfeasible solutions [53, 54].
Notice that, in Figure 5-10, the force constraints are violated in the case of the plant dynamics

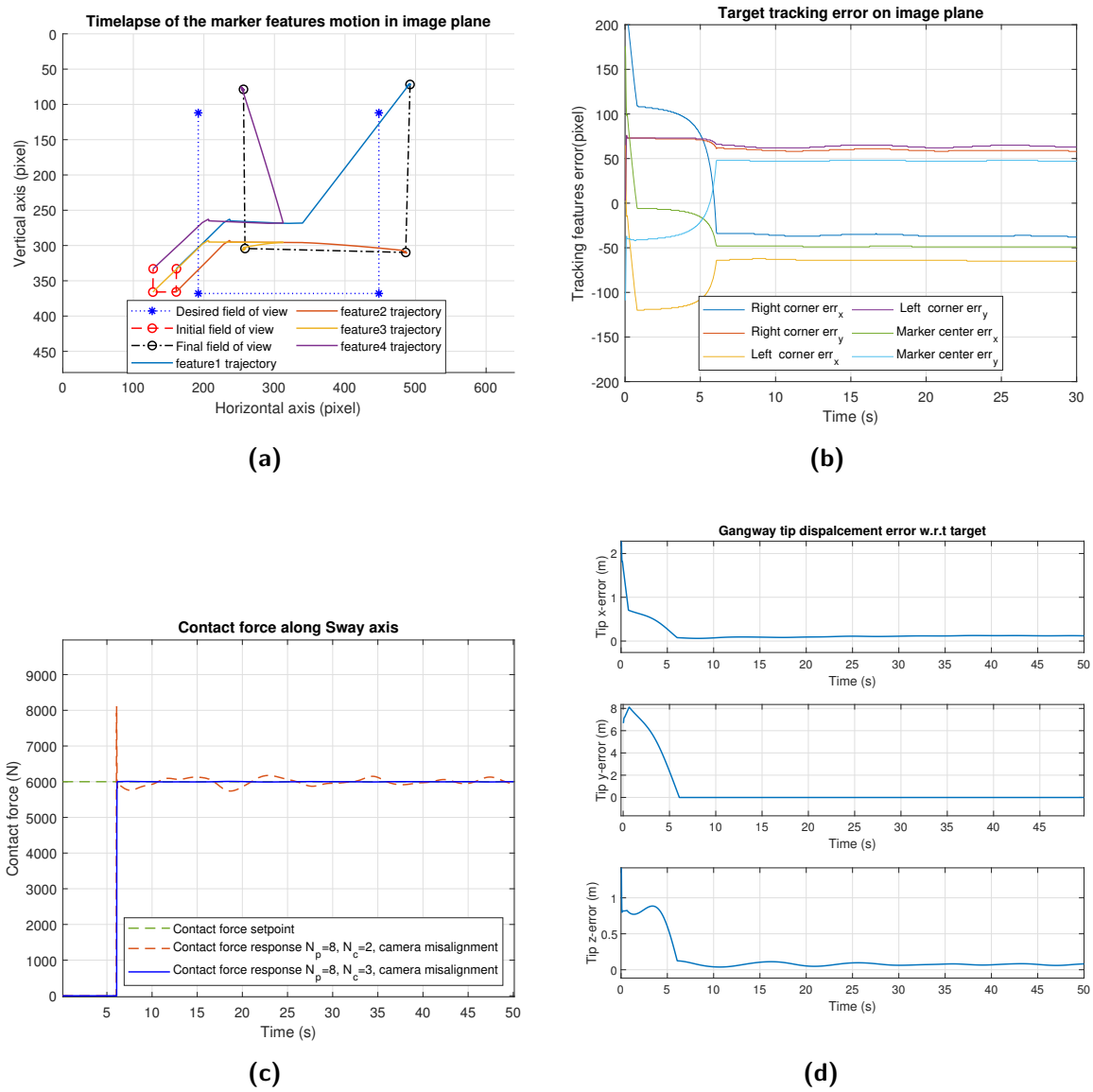

Figure 5-9: (a) and (b) illustrate time-lapse footage of the target (marker) detected features in the field of view over 50 seconds and the corresponding tracking error, respectively. The corresponding contact force response for different N_c values and the error between the tip and the target is depicted in (c) and (d), respectively.

mismatch. However, the performance in the case of $\omega_n = 6.5$ is acceptable since it is nearly within the contact force boundaries (i.e. 4000 to 8000 N).

5-4 Extreme disturbances

Essentially, the target motion is solely the sea-induced motion mapped into the target relative position to the Gangway. The sea-induced motion is a sinusoidal-based motion that varies in the period and amplitude. Thus, in order to guarantee the performance consistency of

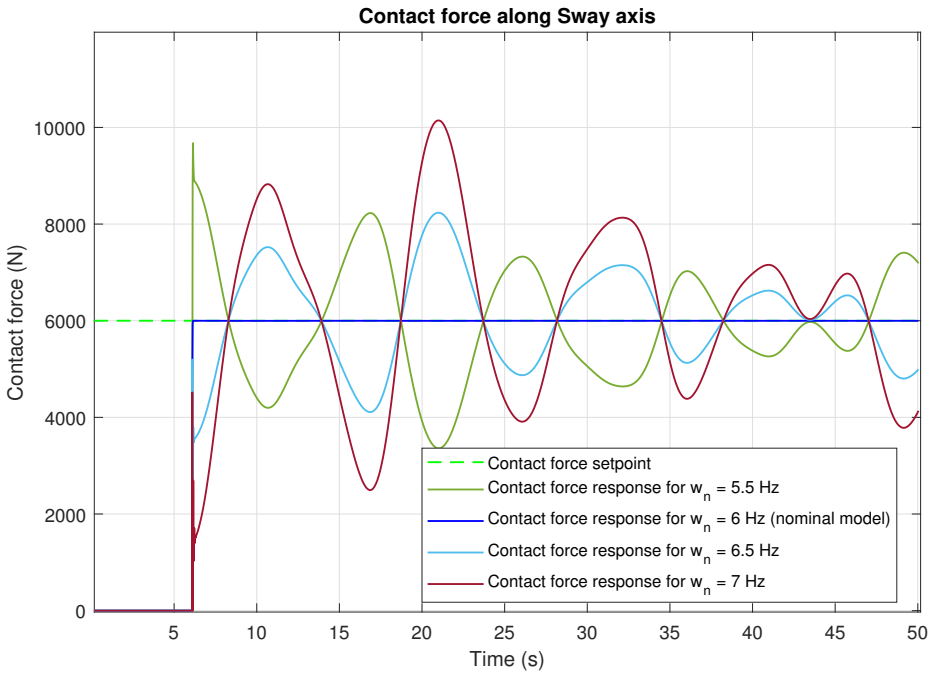

Figure 5-10: The contact force response in case of plant dynamics mismatch.

the proposed control scheme in tracking the target motion, this set of trials is performed. In this set of trials, the disturbance anticipatory property in the MPC was enabled using the provided data set. The prediction horizon was set to $N_p = 8$, and different control horizon values were test $N_c = 3$.

This test is performed for different sea-induced motion conditions, the target pose depicted in Figure 5-7 is considered the nominal case scenario. The induced motion act as a velocity source for the target motion. In Figure 5-11, the second and the third trials employ the same data set of the induced motion amplified by a factor of %150 and %200, receptively. Additionally, the performance is evaluated for a different batch of the induced motion data set.

Figure 5-12, depicts the corresponding contact force response of the aforementioned scenarios. The force response for the nominal case and the fourth case (the different data set case) is nearly identical. However, for the third case, the upper bound (8000 N) for the force response in MPC is violated. Note, this is an extreme case scenario and to ensure the feasibility of the optimisation problem solution the upper bound is this trial was constructed as a soft constraint which allows a near-boundary solution.

5-5 Summary

The performance of the proposed MPC solution for automating the docking procedure is evaluated in this chapter. The controller is first tested for the nominal case with multiple scenarios. Then, tests are preformed against the plant model mismatch. Lastly, the performance is evaluated for a more extreme case in terms of the amplitude of the sea-induced motion.

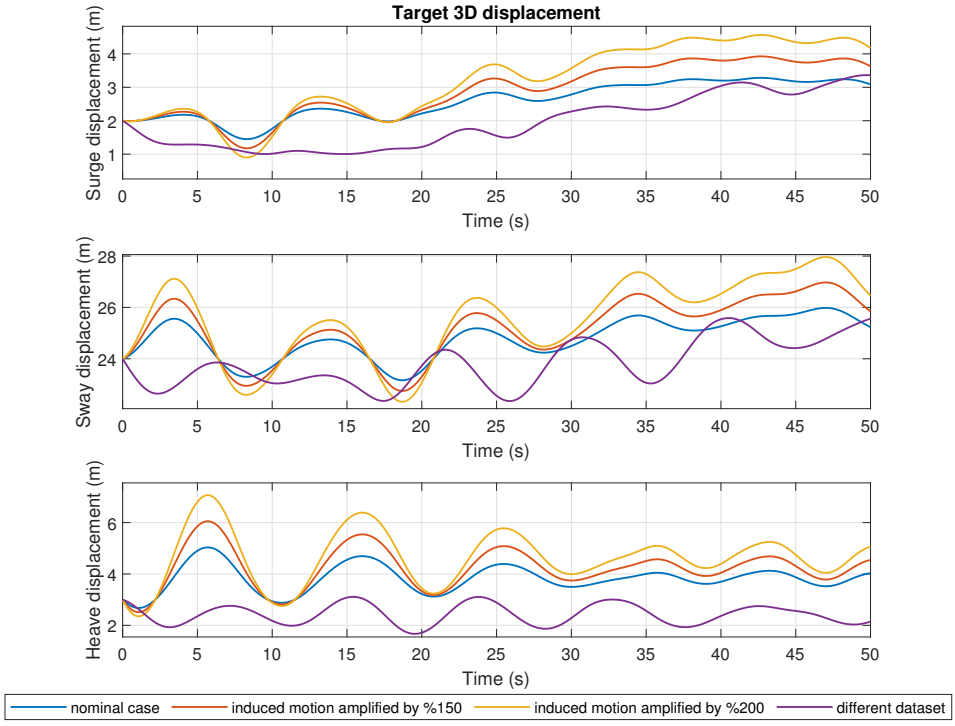

Figure 5-11: The target pose for different induced motion cases.

Figure 5-12: The contact force response for different induced motion cases.

In Section 2-6, the control task requirements for the automated docking are defined. Based on the empirical analysis in this chapter, all the control requirements are fulfilled for the nominal case scenarios and in case of output model mismatch.

Chapter 6

Conclusions and Recommendations

The research objective of this thesis is to develop an automated docking scheme for the gangway system of Bosch. The main purpose is eliminating the operator from the control loop to enhance the safety and efficiency of the system.
According to Bosch, in the current system, the operator relies on his visual perception and vestibular senses to steer the Gangway actuators while the motion of the tip is automatically compensated. Inspired by how the operator estimates the relative motion between the Gangway and the target (i.e. the offshore platform). In Chapter 3, a measurement system is proposed to measure this relative motion. This measurement system comprises a vision sensor, force tip measurements, and Motion Reference Unit (MRU).
The automated docking scheme in this thesis is developed around a nonlinear MPC scheme. The nonlinear MPC employs a nonlinear mathematical model of the Gangway system with the proposed measurement system. This mathematical model is derived for the purpose of simulation and control design. This model embeds an approximation, provided by Bosch, of the joint-level control loop of the Gangway system. Additionally, this model comprises the open-chain kinematic model of the Gangway system and a perspective projection model of the vision sensor.
In this thesis, the proposed control scheme detects and tracks the target in the 2D image plane. Therefore, the control scheme is prone to camera calibrations error. Contrarily to Image-Based Visual Servoing (IBVS) approaches, this proposed scheme enjoys a singularity-free solution in terms of the singularities that are based on image mapping and workspace limitations. Thanks to the employed pinhole camera model and the MPC capability in handling various constraints. Additionally, in Chapter 3, a linear Kalman filter is designed to predict the target position in the image plane in case of a sudden invisibility of the target occurs (i.e. cluttering, outside the field of view). This can safeguard against visual measurements discontinuity which might be problematic from a control perspective.
To gain higher performance, the disturbance anticipatory property in MPC is enabled by forecasting the sea-induced motion. Where a neural network with the NARX topology was designed and trained to acquire a multi-step-ahead prediction model of the induced motion.
In terms of the efficiency, the proposed automated docking scheme performs the docking in 4 to 10 seconds (based on the initial conditions and sea state). Whereas the time it takes the

operator to perform the docking is up to 3 minutes which depends on his/her experience [7]. In Section 2-6, the control task requirements for the automated docking are defined. Based on the empirical analysis in Chapter 5, all the control requirements for the nominal case scenarios are fulfilled. Also, more extreme scenarios are performed to evaluates the overall performance under plant model mismatch and against various sea-induced motion conditions. Overall, in this thesis, the research questions defined in section 1-3, are addressed and answered correspondingly.
Lastly, the work of this thesis is considered as a proof of concept for employing a visions sensor and an MPC scheme to solve the problem of automated docking.

6-1 Future work

The proposed automated docking scheme shows good performance and fulfils the control task requirements. However, there is still a room for improvements and further research. In order to implement the proposed scheme in practice numerous aspects should be further investigated:

- It was assumed that, for the sake of simplicity; no deformations occur in both the vertical and torsional axes of the Gangway. However, according to Bosch, deformations might occur with an observed effect at the tip. One scheme can be proposed is a multi-camera scheme. Where one camera is attached at the tip and another camera is attached on top of the Gangway base with both cameras observe the same target. Similar to the proposed control scheme, the target can be tracked in both camera's field of view, to counteract for tip deformations. This scheme refers to in literature as eye-in-hand/eye-to-hand visual servoing, as presented in [61].

- In Section 1-4, the relative motion hypothesis is made. Where it is assumed that the sea-induced motion that acts on the vessel causes the target (i.e. offshore platform) to move instead. This assumption is made so the Gangway kinematics and dynamics are described in an inertial frame. This hypothesis is yet to be tested by implanting the proposed control scheme on the real system or on a scaled version.

- The employed nonlinear MPC is computationally demanding. While the real-time implementation requirement is out of scope in this thesis. The calculation time for each time step of the control loop takes between 0.05 to 0.3 seconds. This time depends on the optimisation problem complexity (i.e. length of N_p and N_c, sampling time T_s). With a sampling time of $T_s = 0.02$ seconds, the proposed MPC scheme becomes unfeasible to be implemented on the real system. One solution may be proposed is the fast nonlinear MPC scheme in the work of Schindele and Ascheman in [62].

Bibliography

[1] IRENA, "Innovation outlook: Offshore wind," tech. rep., International Renewable Energy Agency, Abu Dhabi, 2016.

[2] "Lewek Falcon," Jun 2019. [Online; accessed 21. Jun. 2019].

[3] "Welcome to Windcat Workboats," Jun 2019. [Online; accessed 21. Jun. 2019].

[4] "Home | German Offshore Wind Energy Foundation," Jun 2019. [Online; accessed 21. Jun. 2019].

[5] B. Walgaard, "Hybrid force-position control of the motion compensated gangway," master thesis, Delft University of Technology, Delft, 2017.

[6] Rexroth, "Motion compensated gangway - system description," tech. rep., Bosch Rexroth, Boxtel, 2017.

[7] Rexroth, "Mcg - basis of design and control," tech. rep., Bosch Rexroth, Boxtel, 2017.

[8] P. Corke, *Robotics, Vision and Control: Fundamental Algorithms In MATLAB® Second, Completely Revised*, vol. 118. Springer, 2017.

[9] R. Szeliski, *Computer Vision: Algorithms and Applications*. Springer Science & Business Media, 2010.

[10] G. J. Garcia, J. A. Corrales, J. Pomares, and F. Torres, "Survey of visual and force/tactile control of robots for physical interaction in spain," *Sensors*, vol. 9, no. 12, pp. 9689–9733, 2009.

[11] G. Allibert, E. Courtial, and F. Chaumette, "Predictive control for constrained image-based visual servoing," *IEEE Transactions on Robotics*, vol. 26, no. 5, pp. 933–939, 2010.

[12] K. M. Lynch and F. C. Park, *Modern Robotics*. Cambridge University Press, 2017.

[13] W. Bierbooms and G. van Bussel, "The impact of different means of transport on the operation and maintenance strategy for offshore wind farms," *Section Wind Energy, Faculty Civil Engineering and Geosciences; Delft University of Technology: Delft, The Netherlands*, 2002.

[14] "Story - ampelmann - motion compensated gangways." https://www.ampelmann.nl/story, note=Accessed: 30-05-2019.

[15] D. GL, "Offshore gangways dnvgl-st-0358," tech. rep., DNV GL, 2017.

[16] M. A. Ranneh, "Automating the docking procedure of an offshore gangway, a literature survey," Master's thesis, Delft University of Technology, Delft, 2017.

[17] D. Newl, "Pedestrian excitation of bridges," *Proceedings of the Institution of Mechanical Engineers, Part C: Journal of Mechanical Engineering Science*, vol. 218, no. 5, pp. 477–492, 2004.

[18] J. Journée, W. Massie, and R. Huijsmans, *Offshore Hydromechanics: Course OE4630*. Delft University of Technology, 2000.

[19] L. H. Holthuijsen, *Waves in oceanic and coastal waters*. Cambridge university press, 2010.

[20] C. S. D. Julio, *Ampelmann: development of the access system for offshore wind turbines*. BOXPress, 2010.

[21] Ø. F. Auestad, J. T. Gravdahl, and T. I. Fossen, "Heave motion estimation on a craft using a strapdown inertial measurement unit," *IFAC Proceedings Volumes*, vol. 46, no. 33, pp. 298–303, 2013.

[22] "Kongsberg Maritime," Jun 2019. [Online; accessed 21. Jun. 2019].

[23] R. Stettner, "Asc workshop presentation," (Aspen, Colorado), NASA, 2008.

[24] J. Gladwin, R. Umamahaeswaran, K. Sivan, and P. Mathias, "Performance evaluation of a vision sensor in 3d virtual environment for rendezvous and docking application," in *Sensing Technology (ICST), 2012 Sixth International Conference on*, pp. 201–206, IEEE, 2012.

[25] S. Kim and A. Billard, "Estimating the non-linear dynamics of free-flying objects," *Robotics and Autonomous Systems*, vol. 60, pp. 1108–1122, 2012.

[26] S. Kim, A. Shukla, and A. Billard, "Catching objects in flight," *IEEE Transactions on Robotics*, vol. 30, no. EPFL-ARTICLE-198748, 2014.

[27] J. Robert, *Autonomous capture of a free-floating object using a predictive approach*. PhD thesis, McGill University, 2008.

[28] S. R. Bista, *Indoor navigation of mobile robots based on visual memory and image-based visual servoing*. PhD thesis, Universite de Rennes 1; Inria Rennes Bretagne Atlantique, 2016.

[29] J. Heikkila, O. Silven, *et al.*, "A four-step camera calibration procedure with implicit image correction," in *cvpr*, vol. 97, p. 1106, Citeseer, 1997.

[30] Z. Zhang, "A flexible new technique for camera calibration," *IEEE Transactions on pattern analysis and machine intelligence*, vol. 22, 2000.

[31] S. S. Tørdal and G. Hovland, "Relative vessel motion tracking using sensor fusion, aruco markers, and mru sensors," 2017.

[32] S. Garrido-Jurado, R. Muñoz-Salinas, F. J. Madrid-Cuevas, and M. J. Marín-Jiménez, "Automatic generation and detection of highly reliable fiducial markers under occlusion," *Pattern Recognition*, vol. 47, no. 6, pp. 2280–2292, 2014.

[33] M. Faessler, E. Mueggler, K. Schwabe, and D. Scaramuzza, "A monocular pose estimation system based on infrared leds," in *Robotics and Automation (ICRA), 2014 IEEE International Conference on*, pp. 907–913, IEEE, 2014.

[34] J. Redmon, S. Divvala, R. Girshick, and A. Farhadi, "You only look once: Unified, real-time object detection," in *Proceedings of the IEEE conference on computer vision and pattern recognition*, pp. 779–788, 2016.

[35] D. Gordon, A. Farhadi, and D. Fox, "Re3: Real-time recurrent regression networks for visual tracking of generic objects," *IEEE Robotics and Automation Letters*, vol. 3, no. 2, pp. 788–795, 2018.

[36] H. C. Kam, Y. K. Yu, and K. H. Wong, "An improvement on aruco marker for pose tracking using kalman filter," in *2018 19th IEEE/ACIS International Conference on Software Engineering, Artificial Intelligence, Networking and Parallel/Distributed Computing (SNPD)*, pp. 65–69, IEEE, 2018.

[37] K. Halvorsen and F. Olsson, "Pose estimation of cyclic movement using inertial sensor data," in *2016 IEEE Statistical Signal Processing Workshop (SSP)*, pp. 1–5, IEEE, 2016.

[38] T. Kautz, B. H. Groh, and B. M. Eskofier, "Augmented motion models for constrained position tracking with kalman filters," in *2016 19th International Conference on Information Fusion (FUSION)*, pp. 849–854, IEEE, 2016.

[39] X. R. Li and V. P. Jilkov, "Survey of maneuvering target tracking. part i. dynamic models," *IEEE Transactions on aerospace and electronic systems*, vol. 39, no. 4, pp. 1333–1364, 2003.

[40] H. H. Helgesen, F. S. Leira, T. I. Fossen, and T. A. Johansen, "Tracking of ocean surface objects from unmanned aerial vehicles with a pan/tilt unit using a thermal camera," *Journal of Intelligent & Robotic Systems*, vol. 91, no. 3-4, pp. 775–793, 2018.

[41] M. Verhaegen and V. Verdult, *Filtering and system identification: a least squares approach*. Cambridge university press, 2007.

[42] S. Sanden, W. Pawlus, G. Hovland, *et al.*, "Real-time 6-dof vessel-to-vessel motion compensation using laser tracker," in *OCEANS 2017-Aberdeen*, pp. 1–9, IEEE, 2017.

[43] C. Liu, J. Xu, J. Zhao, H. Chen, N. Xi, and K. Chen, "Non-vector space visual servoing for multiple pin-in-hole assembly by robot," in *Advanced Robotics and its Social Impacts (ARSO), 2016 IEEE Workshop on*, pp. 134–140, IEEE, 2016.

[44] T. Dallej, N. Andreff, Y. Mezouar, and P. Martinet, "3d pose visual servoing relieves parallel robot control from joint sensing.," in *IROS*, pp. 4291–4296, 2006.

[45] À. Santamaria-Navarro and J. Andrade-Cetto, "Uncalibrated image-based visual servoing," Institute of Electrical and Electronics Engineers, 2013.

[46] P. I. Corke, "Visual control of robot manipulators-a review," in *Visual Servoing: Real-Time Control of Robot Manipulators Based on Visual Sensory Feedback*, pp. 1–31, World Scientific, 1993.

[47] F. Chaumette and S. Hutchinson, "Visual servo control. i. basic approaches," *IEEE Robotics & Automation Magazine*, vol. 13, no. 4, pp. 82–90, 2006.

[48] U. Klank, D. Pangercic, R. B. Rusu, and M. Beetz, "Real-time cad model matching for mobile manipulation and grasping," in *Humanoid Robots, 2009. Humanoids 2009. 9th IEEE-RAS International Conference on*, pp. 290–296, IEEE, 2009.

[49] M. Ulrich, C. Wiedemann, and C. Steger, "Cad-based recognition of 3d objects in monocular images.," in *ICRA*, vol. 9, pp. 1191–1198, 2009.

[50] F. Chaumette and S. Hutchinson, "Visual servo control. ii. advanced approaches [tutorial]," *IEEE Robotics & Automation Magazine*, vol. 14, no. 1, pp. 109–118, 2007.

[51] F. Chaumette and S. Hutchinson, "Visual servoing and visual tracking," in *Handbook of Robotics* (B. Siciliano and O. Khatib, eds.), pp. 563–583, Springer, 2008.

[52] G. Allibert, E. Courtial, and F. Chaumette, "Visual servoing via nonlinear predictive control," in *Visual Servoing via Advanced Numerical Methods*, pp. 375–393, Springer, 2010.

[53] F. Borrelli, A. Bemporad, and M. Morari, "Predictive control," *Online at http://www.mpc.berkeley.edu/mpc-course-material*, 2012.

[54] J. L. Garriga and M. Soroush, "Model predictive control tuning methods: A review," *Industrial & Engineering Chemistry Research*, vol. 49, no. 8, pp. 3505–3515, 2010.

[55] J. M. P. Menezes Jr and G. A. Barreto, "Long-term time series prediction with the narx network: An empirical evaluation," *Neurocomputing*, vol. 71, no. 16-18, pp. 3335–3343, 2008.

[56] T.-N. Lin, C. L. Giles, B. G. Horne, and S.-Y. Kung, "A delay damage model selection algorithm for narx neural networks," *IEEE Transactions on Signal Processing*, vol. 45, no. 11, pp. 2719–2730, 1997.

[57] M. Lazar, W. Heemels, S. Weiland, and A. Bemporad, "Stabilizing model predictive control of hybrid systems," *IEEE Transactions on Automatic Control*, vol. 51, no. 11, pp. 1813–1818, 2006.

[58] H. K. Khalil and J. W. Grizzle, *Nonlinear systems*, vol. 3. Prentice hall Upper Saddle River, NJ, 2002.

[59] A. Bemporad, M. Morari, and N. Ricker, "The mpc simulink library," *Automatic Control Laboratory Physikstrasse*, vol. 3, p. 8092, 2000.

[60] K. Ogata and Y. Yang, *Modern control engineering*, vol. 4. Prentice-Hall, 2002.

[61] G. Flandin, F. Chaumette, and E. Marchand, "Eye-in-hand/eye-to-hand cooperation for visual servoing," in *Proceedings 2000 ICRA. Millennium Conference. IEEE International Conference on Robotics and Automation. Symposia Proceedings (Cat. No. 00CH37065)*, vol. 3, pp. 2741–2746, IEEE, 2000.

[62] D. Schindele and H. Aschemann, "Fast nonlinear mpc for an overhead travelling crane," *IFAC proceedings volumes*, vol. 44, no. 1, pp. 7963–7968, 2011.

Glossary

List of Acronyms

Gangway	Bosch's gangway
DoF	Degree of Freedom
MCG	Motion Compensated Gangway
PLC	Programmable Logic Controller
HNC	Hydraulics-capable Numerical Control
RAO	Response Amplitude Operators
DP	Dynamic Positioning
MPC	Model Predictive Control
MRU	Motion Reference Unite
IMU	Inertial Measurement Unit
PBVS	Pose-Based Visual Seroving
IBVS	Image-Based Visual Seroving
VPC	Visual Predictive Control
IMC	Internal Model Control
LQR	Linear Quadratic Regulator
RNN	Recurrent Neural Network
RMSE	Root Mean Square Error